Mutational analysis of the F plasmid partitioning protein ParA reveals novel residues required for oligomerisation and plasmid maintenance.

Nivedita Mitra[1,2 †], Dipika Mishra[1,2 # †], Irene Aniyan Puthethu[1,2], Ramanujam Srinivasan[1,2 ‡]

[1] School of Biological Sciences, National Institute of Science Education and Research, Bhubaneswar – 752050, India

[2] Homi Bhabha National Institutes (HBNI), Training School Complex, Anushakti Nagar, Mumbai, India 400094

[†] Authors contributed equally to the work

[‡] Corresponding author

e-mail: rsrini@niser.ac.in

[#] Present address:

School of Biological Sciences, University of Edinburgh, Edinburgh EH9 3FF

Running Title: Oligomerisation of ParA in Plasmid segregation.

Keywords: ParA, F plasmid partitioning, oligomerisation

Abstract

Mobile genetic elements such as plasmids play a crucial role in the emergence of antimicrobial resistance. Hence, plasmid maintenance proteins like ParA of the Walker A type cytoskeletal ATPases/ ParA superfamily are potential targets for novel antibiotics. Plasmid partitioning by ParA relies upon ATP-dependent dimerisation and formation of chemophoretic gradients of ParA-ATP on bacterial nucleoids. Though polymerisation of ParA has been reported in many instances, the need for polymerisation in plasmid maintenance remains unclear. In this study, we provide novel insights into the polymerisation of ParA and the effect of polymerisation on plasmid maintenance. We first characterise two mutations, Q351H and W362E, in ParA from F plasmid ($ParA_F$) that form cytoplasmic filaments independent of the $ParBS_F$ partitioning complex. Both mutants fail to partition plasmids, do not bind non-specific DNA and act as super-repressors to suppress transcription from the ParA promoter. Further, we show that the polymerisation of $ParA_F$ requires the conformational switch to the ParA-ATP* state. We identify two mutations, R320A in the C-terminal helix-14 and E375A helix-16 of $ParA_F$, that abolish filament assembly and affect plasmid partitioning. Our results thus suggest a role for higher-order structures or polymerisation of ParA in plasmid maintenance.

38 **INTRODUCTION**

39 Antibiotic resistance is one of the major concerns for the current state of the
40 world health system. The World Health Organization has declared antimicrobial
41 resistance a global priority and identified Enterobacteriaceae as one of the major groups
42 of pathogens as agents against which new antibiotics are urgently needed (Simonsen
43 2018; World Health Organization 2021). Enterobacteriaceae family includes *Klebsiella*
44 and *Escherichia coli*, which are often acquired as hospital-borne infections and fail to
45 respond to antibiotics due to the presence of multidrug resistance genes (Machado et
46 al. 2022; Cerceo et al. 2016; Jalil and Al Atbee 2022). These genes are usually carried
47 on single or low-copy number plasmids and are thought to be the most prevalent means
48 to transfer antibiotic resistance genes across bacterial species (Yong et al. 2009; Phan
49 et al. 2015; Stephens et al. 2020; Meynell et al. 1968; Moran et al. 2015). Thus,
50 understanding plasmid maintenance and spread could be crucial to curtailing the rapid
51 growth of multidrug resistance in bacteria.

52 Stable maintenance of these low copy number plasmids depends upon the
53 functions of cytoskeletal proteins such as the actin homolog ParM (Møller-Jensen et al.
54 2003; van den Ent et al. 2002; Salje et al. 2010), tubulin homolog TubZ (Tinsley and
55 Khan 2006; Anand et al. 2008; Larsen et al. 2007) and the Walker A type Cytoskeletal
56 ATPases (WACA or the ParA superfamily)(Walker et al. 1982; Motallebi-Veshareh et al.
57 1990; Koonin 1993). The ParA family of proteins function to equipartition genetic
58 material, both plasmids and chromosomes, during the bacterial cell cycle program
59 (Ebersbach and Gerdes 2001; Castaing et al. 2008; Le Gall et al. 2016; McLeod et al.
60 2017; Lutkenhaus 2012; Lee and Grossman 2006). The F plasmid is one of the well-

61 studied model systems to understand the mechanisms by which the ParA family of
62 proteins function to ensure equipartitioning of the replicated plasmids into the daughter
63 cells during cell division. $ParA_F$, also known as SopA, is a member of the ParA
64 superfamily, which binds to the nucleotide ATP and localises to the nucleoid within the
65 bacterial cell (Hatano et al. 2007; Castaing et al. 2008; Roberts et al. 2012; Le Gall et al.
66 2016; McLeod et al. 2017; Hirano et al. 1998). $ParA_F$ has an intrinsic ATP hydrolysis
67 activity, which is stimulated several folds upon interaction with the partitioning complex
68 comprising the adapter protein $ParB_F$ (SopB) and the *$parS_F$* (*sopC*) DNA sequence
69 (Ravin et al. 2003; Watanabe et al. 1992; Libante et al. 2001; Ah-Seng et al. 2013; Ogura
70 and Hiraga 1983; Lane et al. 1987; Bouet et al. 2007; Barillà et al. 2005, 2007). Further,
71 upon interaction with the SopBC complex (referred to as $ParBS_F$ hereafter), $ParA_F$
72 exhibits foci formation that occupies the mid-cell, one-quarter or two-thirds positions
73 along the cell length (Niki and Hiraga 1997; Hatano et al. 2007; Hirano et al. 1998).
74 Recent super-resolution imaging also provides direct evidence of nucleoid localisation
75 of ParA (Le Gall et al. 2016; McLeod et al. 2017). Additional *in vitro* reconstitution on
76 DNA carpets and *in vivo* experiments have led to the idea that chemophoretic gradients
77 generated by dimerisation of ParA upon ATP binding and stimulation of ATPase activity
78 by the partitioning complex drive the directional movement of the replicated plasmids to
79 achieve spatial segregation (Vecchiarelli et al. 2013b, 2014; Hu et al. 2015; Hwang et al.
80 2013; Vecchiarelli et al. 2010). Furthermore, the elasticity of the bacterial nucleoid itself
81 has been shown to play a role, leading to the proposal of a DNA-relay model (Lim et al.
82 2014; Surovtsev et al. 2016).

83 However, *in vitro*, $ParA_F$ has also been observed to undergo polymerisation,
84 forming filaments upon interaction with ATP and radial asters in complex with $ParBS_F$
85 (Lim et al. 2005). Such filaments in the presence of $ParBS_F$ were also observed *in vivo*
86 in 15 % of the cells. Further, these filaments have been reported to grow at a rate of
87 0.18 ± 0.05 μm per minute, similar to the rates at which plasmids and chromosomes
88 segregate in bacteria (Lim et al. 2005). Polymeric structures of $ParA_F$ in the presence of
89 ATP have also been observed using electron microscopy (Bouet et al. 2007). Moreover,
90 such filaments and ATP-dependent polymers have also been observed in the case of
91 other ParA (Ringgaard et al. 2009; Hui et al. 2010; Volante and Alonso 2015) and related
92 ParA family members like ParF (Barillà et al. 2007, 2005; Schumacher et al. 2012) and
93 Soj (Leonard et al. 2005, 2004). Interestingly, the polymerisation of such filaments in
94 $ParA_F$ is mediated only by ATP, wherein non-specific DNA is thought to play a role in
95 inhibiting the formation of such polymers (Bouet et al. 2007). On the contrary, the ParA
96 homolog Soj from *Bacillus subtilis*, *Thermus thermophilus* and ParA2 (a member of the
97 Type-Ia superfamily like $ParA_F$) from *Vibrio cholerae* assembles into a higher-order
98 nucleoprotein complex in the presence of DNA (Leonard et al. 2005; Hui et al. 2010;
99 Parker et al. 2021; Leonard et al. 2004; Chodha et al. 2023). Although these early
100 observations supported a cytoskeletal polymerisation-based model for plasmid
101 segregation by $ParA_F$, more recent studies from several ParA members, as mentioned
102 above, have suggested mechanisms of DNA partitioning independent of ParA
103 polymerisation. Models like the diffusion ratchet mechanism (Vecchiarelli et al. 2012;
104 Brooks and Hwang 2017; Hatano and Niki 2010; Hu et al. 2015, 2017), DNA relay
105 mechanism (Lim et al. 2014; Surovtsev et al. 2016), and the Hitch-Hiking models (Le

106 Gall et al. 2016) have indeed questioned the physiological relevance of ParA
107 polymerisation.

108 Interestingly, Pogliano and colleagues had reported a spontaneous mutant of
109 $ParA_F$ (M315I Q351H) that stabilised the polymers in *E. coli* cells (Lim et al. 2005).
110 Further, we had earlier carried out an extensive mutational analysis of the C-terminal
111 region in $ParA_F$ and found a significant role for the C-terminal helix in plasmid
112 maintenance (Mishra et al. 2022). More recently, a cryo-EM study of filaments formed
113 by ParA from *Vibrio cholerae*, the $ParA2_{Vc}$ protein, has been suggested to involve the C-
114 terminal helix of the protein (Parker et al. 2021). Thus, these recent cryo-EM studies
115 prompted us to revisit the role of polymerisation in ParA function. Here, we report that
116 the C-terminal helix 14 and helix 16 play a significant role in stabilising the SopA
117 polymers. We first show that a single mutation (Q351H) is sufficient to recapitulate the
118 cytoplasmic filaments seen in $ParA_F$ M3154I Q351H (SopA1). We also report another
119 mutant of $ParA_F$, W362E, which assembles into similar polymers in the cytoplasm of *E.*
120 *coli* cells, suggesting that the mutants act to stabilise the $ParA_F$ polymers *in vivo*. We
121 show that while $ParA_F$ Q351H and W362E retain their ability to interact with the $ParA_F$
122 promoter region to act as super-repressors, the assembled filaments are not nucleoid-
123 associated. Further, $ParA_F$ Q351H strongly induces polymerisation of the wild-type
124 $ParA_F$ when co-expressed. Moreover, using various mutants $ParA_F$ in the conserved
125 K120 residue in the Walker A motif, we find that polymerisation of $ParA_F$ Q351H and
126 W362E requires ATP binding and depends upon the conformational change to the
127 ParA-ATP* state. Finally, we show that polymerisation is completely abolished when we
128 change a charged residue, E375, in the C-terminal helix 16 or R320 in helix 14 to

129 alanine. While $ParA_F$ E375A and $ParA_F$ R320A retain weak transcriptional activity in
130 response to the $ParBS_F$ complex, the mutants fail to maintain plasmids in cells stably.
131 Thus, our studies here highlight a role for helix 14 and the C-terminal helix 16 in
132 polymerisation of $ParA_F$ and are suggestive of a requirement of higher order structures
133 (oligomerisation) for co-operative binding of $ParA_F$ to DNA and F-plasmid segregation
134 functions.

135 **RESULTS**

136 **Mutations in $ParA_F$ Q351 or W362 stabilise $ParA_F$ polymers and impair DNA**
137 **partitioning**

138 We and others have earlier shown that a C-terminal GFP fusion to $ParA_F$ is fully
139 functional for plasmid partitioning, localises to the bacterial nucleoid and forms
140 oscillating foci in the presence of $ParBS_F$ complex (Lim et al. 2005; Bouet et al. 2007;
141 Hatano et al. 2007; Ah-Seng et al. 2013; Le Gall et al. 2016; Mishra et al. 2022). $ParA_F$-
142 GFP and its variants were expressed from the weakened P_{trc} promoter, while *parBS*$_F$
143 was carried on a mini-F plasmid, pDAG198, that lacked $ParA_F$ (*ΔparA*$_F$*, parBS*$^+$) under
144 the constitutive $P_{LtetO-1}$ promoter (Castaing et al. 2008). In the presence of the *parBS*$_F$,
145 the wild type $ParA_F$-GFP (SopA) formed foci or appeared as a haze, consistent with
146 earlier reports suggesting nucleoid association **(Fig. 1A)**. On the contrary, $ParA_F$ M315I
147 Q351H-GFP (called SopA1) formed filament structures in the cell **(Fig. 1A)** as reported
148 previously (Lim et al. 2005). To test if the Q351H mutation, instead of the double
149 mutations, was sufficient to trigger the polymerisation of $ParA_F$, we generated $ParA_F$
150 Q351H-GFP and expressed it in *E. coli* from the same weakened P_{trc} promoter. $ParA_F$

151 Q351H-GFP also assembled into cytoplasmic filaments similar to that formed by $ParA_F$
152 M315I Q351H-GFP, showing that the mutation in the residue Q351 was sufficient to
153 induce polymerisation of $ParA_F$ **(Fig. 1A).** During the course of our studies on the role of
154 the C-terminal helix on $ParA_F$ function (Mishra et al. 2022), we identified another
155 mutation, W362E, which likewise resulted in the assembly of $ParA_F$-GFP into
156 cytoplasmic filaments **(Fig. 1A)**. In the case of $ParA_F$ M315I Q351H, 56.5 % ± 11.27
157 (95% CI, n=3, at least 100 cells were counted for each experiment) formed cytoplasmic
158 filaments. Further, 41.3 % ± 14.8 (95% CI, n=3; at least 100 cells were counted for each
159 experiment) of the cells in the case of $ParA_F$ Q351H contained filaments, while in the
160 case of $ParA_F$ W362E, 38.0 % ± 17.9 (95% CI, n=3; at least 100 cells were counted for
161 each experiment) of the cells contained filaments in presence of $parBS_F$ complex **(Fig.**
162 **1B)**.

163 The cytoplasmic filaments assembled by $ParA_F$ M315I Q351H-GFP have been
164 reported to be less dynamic as compared to the WT-$ParA_F$ and fail to support F plasmid
165 maintenance (Lim et al. 2005). We, therefore, tested whether the assembly of $ParA_F$
166 Q351H and W362E into polymers also resulted in the loss of mini-F plasmids from cells
167 and carried out plasmid stability assays using the two-plasmid system (Ah-Seng et al.
168 2013; Mishra et al. 2022). $ParA_F$-GFP and its variants were expressed from the
169 weakened P_{trc} promoter and a mini-F plasmid lacking $ParA_F$ but containing $parBS_F$
170 under the constitutive $P_{LtetO-1}$ promoter (mini-F Cam^R $P_{LtetO-1}$*::ΔparA*$_F$, *parBS*$^+$; Castaing
171 et al. 2008) constituted the second plasmid whose maintenance was tested. As would
172 be expected, in the presence of wild-type $ParA_F$-GFP, mini-F plasmids were maintained
173 stably, whereas a loss rate of 4.3 % ± 0.32 (SD, n=3; at least 400 colonies were tested

174 for each experiment) per generation was observed in the absence of $ParA_F$. The mini-F
175 plasmid loss rates in cultures carrying $ParA_F$ mutants Q351H and W362E were 3.1 % ±
176 0.80 (SD, n=3; at least 400 colonies were tested for each experiment) and 3.7 % ± 0.40
177 (SD, n=3; at least 400 colonies were tested for each experiment) respectively, which
178 was comparable to those lacking $ParA_F$ **(Fig. 1C)**. $ParA_F$ M315I Q351H-GFP (SopA1)
179 also exhibited plasmid loss from the cultures as reported earlier (Lim et al. 2005) at the
180 rate of 3.3 % ± 0.33 (SD, n=3; at least 400 colonies were tested for each experiment),
181 showing that these $ParA_F$ mutants that assemble into stable polymers are impaired in
182 partitioning plasmids.

183

184 **$ParA_F$ Q351H and $ParA_F$ W362E or W362A assemble into polymers in the absence**
185 **of *$parBS_F$***

186 Earlier reports have suggested that ParB influences the polymerisation of $ParA_F$
187 (Bouet et al. 2007). We thus tested if $ParA_F$ M315I Q351H, $ParA_F$ Q351H and $ParA_F$
188 W362E assembled into cytoplasmic filaments in the absence of *$parBS_F$*. Cytoplasmic
189 filaments of $ParA_F$ M315I Q351H-GFP, $ParA_F$ Q351H-GFP and $ParA_F$ W362E-GFP
190 were observed in the absence of $ParBS_F$ as well **(Fig. 2A)**, showing that the
191 polymerisation of these $ParA_F$ mutants were independent of the partitioning complex.
192 We also substituted W362 with a non-polar amino acid, alanine (W362A) and found that
193 $ParA_F$ W362A-GFP also assembled into polymers similar to those formed by $ParA_F$
194 M315I Q351H, $ParA_F$ Q351H, and $ParA_F$ W362E **(Fig. 2A)**. Moreover, in the absence of
195 *$parBS_F$*, quantification of the number of cells with filaments showed no significant

196 differences between the various $ParA_F$ mutants **(Fig. 2B)**. While cells expressing $ParA_F$
197 M315I Q351H-GFP showed 39.2 % ± 3.37 (95% CI, n=3; at least 100 cells were
198 counted for each experiment) of cells containing filaments, $ParA_F$ Q351H-GFP and
199 $ParA_F$ W362E-GFP resulted in 48.7 % ± 9.46 (95% CI, n=3; at least 150 cells were
200 counted for each experiment) and 42.80 % ± 8.23 (95% CI, n=3; at least 150 cells were
201 counted for each experiment) of cells having filaments, respectively **(Fig. 2B)**. The
202 percentage of cells having filaments in the case of $ParA_F$ W362A was 53.8 % ± 15.12
203 (95% CI, n=3; at least 150 cells were counted for each experiment) **(Fig. 2B)**. Further,
204 $ParA_F$ Q351H and W362E filaments showed a mean length of 0.88 μm ± 0.19 (95% CI,
205 n=3; number of cells counted were > 73 and < 121) and 0.71 μm ± 0.14 (95% CI, n=3;
206 number of cells counted were > 59 and < 99) respectively **(Fig. 2C)**.
207 Fission yeast (*Schizosaccharomyces pombe*) has been used as a heterologous
208 host to study the assembly of cytoskeletal proteins of bacteria and chloroplast
209 (Srinivasan et al. 2007, 2008; Pande et al. 2022; TerBush et al. 2018; TerBush and
210 Osteryoung 2012). We thus tested if these $ParA_F$ mutants (M315I Q351H, Q351H and
211 W362E) assembled to filaments in fission yeast as well. We expressed $ParA_F$ M315I
212 Q351H, $ParA_F$ Q351H or $ParA_F$ W362E as C-terminal GFP fusions in fission yeast using
213 the medium-strength thiamine repressible promoter *nmt41/42* (Basi et al. 1993). We
214 observed that, while $ParA_F$-GFP was localised to the nucleus, probably owing to the
215 nsDNA binding activity, $ParA_F$ M315I Q351H-GFP, $ParA_F$ Q351H-GFP and $ParA_F$
216 W362E-GFP assembled into polymeric structures in the cytoplasm of *S. pombe* **(Fig.
217 2D)**. Interestingly, the filament length spanned the length of *S. pombe* cells, suggesting
218 that the limited filament length observed in *E. coli* was possibly a result of either the

219 physical limit of cell length or the amount of protein available for polymerisation. These
220 observations further suggest that the polymerisation of these mutants was intrinsic to
221 $ParA_F$ and that these filaments were formed independent of any host factor specific to
222 assembly in bacteria. Taken together, these results suggest that the mutations in the
223 residues Q351 and W362 result in the formation of stable polymers of $ParA_F$, and the
224 assembly into cytoplasmic filaments is independent of the $ParBS_F$ partitioning complex.
225

226 **Q351 and W362 influence non-specific DNA binding**

227 $ParA_F$-mediated plasmid partitioning is majorly dependent on the nucleoid
228 association of $ParA_F$-ATP dimers and the formation of the chemophoretic gradient
229 through which the ParB-*parS* plasmid complex migrates. We had earlier shown that the
230 last C-terminal helix played a role in nsDNA binding and plasmid partitioning. Both
231 Q351H and W362E in $ParA_F$ map to the C-terminal region, and it was thus imperative
232 for us to test if these filament-forming mutants were also impaired in interaction with
233 non-specific DNA. The localisation of the filaments formed by these mutant proteins was
234 thus determined by live-cell imaging in conjunction with the nucleoid stain DAPI and the
235 membrane marker FM 4-64. $ParA_F$ Q351H-GFP and $ParA_F$ W362E-GFP filaments often
236 seemed to localise between the nucleoid and the membrane and appeared not to be co-
237 localised with DNA (**Fig. 3A**). Further 3D structured illumination microscopy (3D-SIM) of
238 cells expressing $ParA_F$ Q351H-GFP **(Fig. 3B i)** and $ParA_F$ W362E-GFP **(Fig. 3B ii)**
239 showed that the spatial localisation of the polymers were clearly distinct from the
240 nucleoid, suggesting that these filaments were cytoplasmic and were not associated

241 with the nucleoid. **(Fig. 3B i and ii)**. In order to better visualise DNA-free regions and
242 determine if the polymers were indeed localised to DNA-free regions and not bound to
243 the nucleoid, we inhibited cell division using cephalexin for a short duration of 30
244 minutes and condensed nucleoids using chloramphenicol, stained them with DAPI and
245 carried out live-cell imaging. The $ParA_F$ Q351H-GFP and $ParA_F$ W362E-GFP filaments
246 were invariably localised to the nucleoid-free regions of the cell **(Fig. 3C)**, and we did
247 not find any co-localisation of filaments with the nucleoid. On the contrary, $ParA_F$-GFP
248 was seen to be entirely co-localised with the nucleoid, as expected **(Fig. 3C)**.
249

250 **Co-expression of filament-forming mutants can induce polymerisation of wild-**
251 **type $ParA_F$-GFP**

252 Earlier studies have shown that $ParA_F$ M315 Q351H (SopA1) can co-assemble with
253 $ParA_F$-GFP and induce the formation of $ParA_F$-GFP filaments. To further test if $ParA_F$
254 Q351H and $ParA_F$ W362E can similarly induce polymerisation of wild-type $ParA_F$-GFP,
255 which are otherwise localised to the nucleoid, we resorted to in vivo imaging of a two-
256 plasmid system. We expressed the wild-type $ParA_F$-GFP fusion from the P_{trc} promoter
257 (pDSW210 vector, Amp^R) as described above and simultaneously expressed versions
258 of $ParA_F$ Q351H or $ParA_F$ W362E lacking the fluorescent protein tag from the highly
259 regulated arabinose promoter (pBAD33 vector, Cm^R). Upon co-expression of untagged
260 wild-type $ParA_F$ from the pBAD33 vector, $ParA_F$-GFP was found localised to the
261 nucleoid as expected **(Fig. 4A)**. However, $ParA_F$-GFP assembled into polymers in cells
262 co-expressing untagged $ParA_F$ Q351H **(Fig. 4A)**, suggesting that $ParA_F$ Q351H co-
263 assembled with wild-type $ParA_F$-GFP and stabilised $ParA_F$ in its polymeric form *in vivo*.

264 On the contrary, $ParA_F$ W362E only weakly induced polymerisation of $ParA_F$-GFP and
265 most of the $ParA_F$ remained nucleoid-associated **(Fig. 4A)**. Further, the polymers
266 assembled by wild-type $ParA_F$-GFP were more clearly visualised upon preventing cell
267 division by treatment of cells with cephalexin (**Fig. 4B)**. Thus, using co-expression of
268 WT-$ParA_F$-GFP and untagged versions of $ParA_F$ mutants and imaging, we show that the
269 mutants $ParA_F$ Q351H and $ParA_F$ W362E can co-polymerise with wild-type $ParA_F$ and
270 sequestered into the polymeric form. Our results here further support the premise that
271 wild-type $ParA_F$ has the property to assemble into higher-order oligomers, and these
272 mutations (Q351H and W362E) resulted in the polymerisation of $ParA_F$ *in vivo*.
273

274 **Continuous protein synthesis is required to maintain $ParA_F$ filaments**

275 We next attempted to visualise the polymerisation dynamics of $ParA_F$ Q351H and
276 $ParA_F$ W362E. However, we could rarely capture the phenomenon of foci/ spot to
277 filament formation in our time-lapse images. The increment in the length could not be
278 discerned, probably owing to limiting protein levels due to the weak promoter used
279 (pDSW210; Weiss et al., 1999) and cell division-induced dilution effects. Therefore, we
280 resorted to cephalexin treatment of cells, which inhibited cell division, to monitor
281 filament growth in the presence of IPTG. We were able to monitor filament elongation in
282 these non-dividing cells and were able to capture the growth of the polymers assembled
283 by $ParA_F$ Q351H-GFP **(Fig. 5A)** and $ParA_F$ W362E-GFP **(Fig. 5B)** in our time-lapse
284 experiments.

285 Moreover, we had serendipitously observed that cells containing $ParA_F$ W362E-
286 GFP filaments exhibited diffuse cytoplasmic fluorescence when placed on LB agarose

287 pads lacking IPTG for extended periods **(Supplementary Fig. S1**). Further, we also
288 observed that $ParA_F$ Q351H-GFP exhibited shortening or loss of $ParA_F$ filaments within
289 20-minutes on LB agarose pads lacking IPTG **(Fig. 5C)**. The depolymerisation of $ParA_F$
290 filaments in the absence of IPTG suggested that the maintenance of polymers required
291 continuous protein synthesis. To determine if the persistence of $ParA_F$ filaments
292 depended upon continual protein synthesis, we prevented further induction of protein
293 and blocked protein synthesis in cells expressing $ParA_F$ filaments and carried out time-
294 lapse microscopy. We first grew cultures carrying pDSW210-$ParA_F$ Q351H or
295 pDSW210-$ParA_F$ W362E with IPTG to induce polymerisation. We then carried out time-
296 lapse imaging of these cells placed on IPTG containing agarose pads and compared
297 them with cells imaged on agarose pads containing chloramphenicol and glucose, but
298 lacking IPTG. We added chloramphenicol (Cm), a protein synthesis inhibitor, to prevent
299 further protein synthesis and glucose (Glu) to completely repress $ParA_F$ expression from
300 the weakened P_{trc} promoter. Time-lapse imaging of $ParA_F$ Q351H-GFP **(Fig. 5D)** and
301 $ParA_F$ W362E-GFP **(Fig. 5E)** in the presence of Glu + Cm **(Fig. 5D i and 5E i)** or IPTG
302 **(Fig. 5D ii and 5E ii)** confirmed that the filaments indeed underwent depolymerisation in
303 the absence of continued protein synthesis within a period of approximately 20 minutes
304 **(Fig. 5 D i and E i)**. These results suggest that both $ParA_F$ Q351H and W362E require a
305 critical concentration of protein to assemble into polymers and there exists a
306 cytoplasmic pool of unpolymerised subunits as well in addition to the filaments
307 observed.

308 **$ParA_F$ Q351H and $ParA_F$ W362E act as super-repressors of the *$parAB_F$* promoter**

309 $ParA_F$ is known to weakly repress transcription from its own promoter by binding
310 to the four operator sequences. A winged helix-turn-winged helix (WTH) domain that is
311 distinct from the nsDNA binding residues is responsible for promoter sequence
312 recognition and binding (Hirano et al. 1998; Lemonnier et al. 2000; Libante et al. 2001;
313 Komai et al. 2011; Yates et al. 1999; Mori et al. 1989; Bouet et al. 2007; Ah-Seng et al.
314 2009; Ravin et al. 2003; Hayes et al. 1994; Abeles et al. 1985). This auto-regulatory
315 activity of $ParA_F$ is very weak but is enhanced in the presence of the $ParBS_F$ complex.
316 (Ravin et al. 2003; Mori et al. 1989; Hirano et al. 1998; Libante et al. 2001). While the
317 filaments formed by $ParA_F$ Q351H and $ParA_F$ W362E were not nucleoid-associated, we
318 tested if $ParA_F$ Q351H and $ParA_F$ W362E (presumably the cytosolic subunits) could at
319 least bind the specific DNA sequences in the promoter region of $ParA_F$ and act to
320 repress gene expression. In order to do so, we resorted to using an *in vivo* reporter
321 assay based on *lacZ* fusion to the P_{parF} promoter and utilised the *E. coli* DLT1127
322 strain (PparF::lacZ; Ravin and Lane 1999). As reported earlier, we made use of $ParA_F$
323 constructs that carried a stop codon between $ParA_F$ and GFP (Mishra et al. 2022) **(Fig.
324 6A)**. We transformed $ParA_F$ or the mutant plasmids into the DLT1127 strain of *E. coli*
325 carrying a mini-F plasmid containing $ParBS_F$ region but lacking $ParA_F$ (mini-F $\Delta parA_F$
326 $parBS^+$) and assayed for promoter repression by spotting serial dilutions of the cultures
327 on X- Gal + IPTG plates. In the presence of $ParBS_F$, although $ParA_F$ and both the
328 mutants (Q351H and W362E) repressed the expression of LacZ from the P_{parF}
329 promoter, the extent of repression by $ParA_F$ Q351H and $ParA_F$ W362E appeared to be
330 stronger **(Fig. 6B; top panel)**. However, in the absence of the $ParBS_F$ complex, while
331 $ParA_F$ showed a reduced ability to repress LacZ expression as expected, $ParA_F$ Q351H

332 and $ParA_F$ W362E continued to strongly repress the expression of LacZ (**Fig. 6B,**
333 **bottom panel**). Further, quantification of the LacZ expression levels by β-galactosidase
334 assays using ONPG as a substrate (**Figure 9** below) also showed that the repressor
335 function of $ParA_F$ Q351H and $ParA_F$ W362E were not responsive to the presence of the
336 $ParBS_F$ complex. Expression of LacZ was repressed by 74.27 % ± 3.22 (SD, n = 3) and
337 70.85 % ± 4.95 (SD, n = 3) by $ParA_F$ Q351H in the presence and absence of $ParBS_F$
338 complex, respectively. Repression of LacZ by $ParA_F$ W362E was weaker and showed
339 44.60 % ± 8.87 (SD, n = 3) and 44.03 % ± 1.16 (SD, n = 3) in the presence and
340 absence of $ParBS_F$ complex, respectively. On the contrary, $ParA_F$ showed a significant
341 repression of 74.04 % ± 2.05 (SD, n = 3) in the presence of the $ParBS_F$ complex
342 compared to a mere 6.40 % ± 9.83 (SD, n = 3) in its absence. These results suggested
343 that the repression of the $ParA_F$ promoter activity by $ParA_F$ Q351H and $ParA_F$ W362E
344 resulted in a so-called super-repressor activity of $ParA_F$ independent of the $ParBS_F$
345 complex.

346 **Polymerisation is an ATP-dependent process and requires the conformational**
347 **change to $ParA_F$-ATP* state**

348 *In vitro* studies of $ParA_F$ and several ParA homologs have shown that polymerisation
349 was strictly an ATP-dependent process (Lim et al. 2005; Leonard et al. 2005; Bouet et
350 al. 2007; Parker et al. 2021). Thus, we wanted to test if the observed *in vivo*
351 polymerisation of $ParA_F$ W362E-GFP was dependent upon ATP binding. The residue
352 K120 in $ParA_F$ has been reported to be essential for ATP binding and hydrolysis
353 (Libante et al. 2001; Hatano et al. 2007). Changing this residue to glutamic acid (E) in

354 $ParA_{P1}$ has been shown to specifically affect ATP binding (Vecchiarelli et al. 2013a;
355 Chodha et al. 2023; Fung et al. 2001; Davis et al. 1996). We, therefore, generated $ParA_F$
356 double mutants ($ParA_F$ K120E W362E-GFP) and assessed their ability to form polymers
357 in *E. coli*. As compared to the single mutant $ParA_F$ W362E **(Fig. 7A)**, the double
358 mutation resulted in a complete loss of polymerisation and exhibited diffuse
359 fluorescence of $ParA_F$-GFP over the entire cytoplasm of the cell, underlining the role of
360 ATP binding in the polymerisation of these $ParA_F$ mutants **(Fig. 7A)**. These results
361 therefore suggest that the assembly of $ParA_F$ W362E-GFP into cytoplasmic filaments
362 was strictly an ATP dependent process.

363 $ParA_F$ has been proposed to undergo a conformational state change upon ATP-
364 binding (Libante et al. 2001; Vecchiarelli et al. 2010; Zhang and Schumacher 2017;
365 Caccamo et al. 2020; Dobruk-Serkowska et al. 2012; Baxter et al. 2020). Since
366 polymerisation of $ParA_F$ W362E-GFP was ATP-binding dependent, we next sought to
367 determine if polymerisation required ATP hydrolysis and the conformational change to
368 the $ParA_F$-ATP* state. Different mutations in the same lysine residue (K120) have been
369 reported to have different effects on $ParA_{P1}$ (Fung et al. 2001; Davis et al. 1996;
370 Vecchiarelli et al. 2013a). In $ParA_F$, both K120R and K120Q have been shown to
371 interact with ATP but fail to attain the $ParA_F$-ATP* conformational state, but only $ParA_F$
372 K120Q still retains its intrinsic ATP-hydrolysis activity similar to that of $ParA_F$ (Ah-Seng
373 et al. 2013; Libante et al. 2001; Le Gall et al. 2016). Therefore, we examined the effects
374 of these ATP mutant variants (K120R and K120Q) on the polymerisation of $ParA_F$
375 W362E-GFP. Both the double mutants, $ParA_F$ K120R W362E and $ParA_F$ K120Q
376 W362E, failed to assemble into polymers and exhibited only diffuse cytoplasmic

377 fluorescence, suggesting that a conformational change to $ParA_F$-ATP* state but not ATP
378 hydrolysis was necessary for the stabilisation of $ParA_F$ filaments. We also substituted
379 K120 with alanine in $ParA_F$ W362E-GFP, and surprisingly, we observed that $ParA_F$
380 K120A W362E-GFP was still able to assemble into polymers **(Fig. 7A)**. Furthermore,
381 the percentage of cells having cytoplasmic filaments or the average filament length in
382 the case of $ParA_F$ K120A W362E-GFP were not significantly different than for $ParA_F$
383 W362E-GFP **(Fig. 7 B and C)**. Thus, in contrast to the K120R and K120Q mutations,
384 the K120A mutation did not prevent the polymerisation of $ParA_F$ W362E-GFP.

385 The conformational change to the $ParA_F$-ATP* state is essential for the nucleoid
386 association and formation of $ParA_F$ foci in the presence of the $ParBS_F$ complex (Libante
387 et al. 2001). Accordingly, $ParA_F$ K120R and $ParA_F$ K120Q are defective in foci formation
388 (Hatano et al. 2007; Hu et al. 2021). We therefore reasoned that if $ParA_F$ K120A
389 retained the ability to undergo the conformational change to the $ParA_F$-ATP* state,
390 $ParA_F$ K120A-GFP should assemble into foci like that of wild-type $ParA_F$-GFP in the
391 presence of $ParBS_F$ complex **(Fig. 7D)**. Consistently, we observed that $ParA_F$ K120A-
392 GFP formed foci over the nucleoid region like $ParA_F$-GFP. Quantification of the
393 distribution of foci per cell showed only subtle differences between $ParA_F$-GFP and
394 $ParA_F$ K120A-GFP **(Fig. 7E)**. Taken together, these results suggest that $ParA_F$ K120A
395 undergoes the conformational change to $ParA_F$-ATP* state and that the assembly into
396 cytoplasmic filaments by the $ParA_F$ W362E-GFP requires the formation of $ParA_F$-ATP
397 dimers and the conformational change to its $ParA_F$-ATP* state.

398 **Polar residues E375 in the last C-terminal helix and R320 in helix 14 play a role in**
399 **polymerisation and plasmid maintenance function of $ParA_F$**

400 Recent cryo-electron microscopic studies of $ParA2_{Vc}$ have revealed a polymeric
401 structure of ParA bound to DNA, and the last C-terminal helix 16 constituted an
402 important oligomer interface in the nucleoprotein filament complex (Parker et al. 2021).
403 Moreover, we had earlier reported that the last C-terminal helix was essential for
404 function in $ParA_F$. In a study involving multiple point mutations of the charged residues
405 in the C-terminal helix 16 of $ParA_F$, we had found that E375A impacted nucleoid
406 localisation of $ParA_F$ *in vivo* (Mishra et al. 2022). Therefore, we introduced E375A into
407 $ParA_F$ W362E-GFP and tested their effects on the polymerisation of $ParA_F$. Further, we
408 carried out mutational studies in the conserved residues proximal (e.g. R320 and K329)
409 to the previously identified nsDNA binding residues and tested their effects on $ParA_F$
410 W362E-GFP. The double mutants, $ParA_F$ W362E E375A-GFP and $ParA_F$ W362E
411 R320A-GFP, failed to assemble into polymers and exhibited diffuse fluorescence
412 throughout the cell **(Fig. 8A)**, suggesting that E375 in the last C-terminal helix and R320
413 might be involved in the polymerisation of $ParA_F$. Quantification of total fluorescence
414 intensity in the cells expressing $ParA_F$ W362E-GFP, $ParA_F$ W362E E375A-GFP or
415 $ParA_F$ W362E R320A-GFP did not show any significant differences, suggesting that the
416 protein levels were similar in these cells **(Fig. 8B)** and that the mutations R320A and
417 E375A affected polymerisation of $ParA_F$.

418 Next, in order to ascertain if polymerisation and, thereby, residues E375 and
419 R320 were important for $ParA_F$ function, we determined if plasmid maintenance was
420 affected by the E375A and R320A mutations. As described above, we utilised the two-

421 plasmid system, wherein we assessed the stability of the mini-F plasmid (pDAG198;
422 *ΔparA$_F$, parBS$^+$*) and expressed ParA$_F$ or its variants from P$_{trc}$ promoter in the
423 pDSW210 vector. We had earlier shown that ParA$_F$ E375A-GFP exhibited mild plasmid
424 loss compared to ParA$_F$-GFP (Mishra et al. 2022). Consistently, we found that ParA$_F$
425 E375A-GFP showed a plasmid loss of 1.6 ± 0.55 (SD, n = 3, at least 400 colonies were
426 tested for each experiment) per generation **(Fig. 8C)**. ParA$_F$ R320A-GFP showed a
427 higher plasmid loss of 3.6 ± 0.33 (SD, n = 3, at least 400 colonies were tested for each
428 experiment) and comparable to the plasmid loss in cultures lacking ParA$_F$ [3.4 ± 0.1
429 (SD, n = 3, at least 400 colonies were tested for each experiment)] **(Fig. 8C)**. Further,
430 we had also shown that ParA$_F$ E375A-GFP did not bind DNA and failed to form foci in
431 the presence of ParBS$_F$ complex (Mishra et al. 2022). We thus tested if ParA$_F$ R320A-
432 GFP also behaved similarly and assessed its localisation in both the presence and
433 absence of the ParBS$_F$ complex. We used a strain of *E. coli* expressing HupA-mCherry
434 to visualise the nucleoid. As a control, we also used ParA$_F$-GFP, and as expected, it
435 was found to be localised on the nucleoid in the absence of the ParBS$_F$ complex.
436 Consistent with our results, ParA$_F$ E375A-GFP was found to be evenly distributed
437 throughout the cell in the absence of the ParBS$_F$ complex **(Fig. 8D)**. On the contrary,
438 ParA$_F$ R320A-GFP showed mild localisation to the nucleoid, but unlike ParA$_F$-GFP,
439 fluorescence was found to be distributed in nucleoid free regions of the cell as well **(Fig.
440 8D)**. Further, in the presence of the ParBS$_F$ partitioning complex, only ParA$_F$-GFP
441 exhibited foci formation and both ParA$_F$ E375A and ParA$_F$ R320A resulted in
442 predominantly diffuse fluorescence throughout the cytoplasm of the cell. However,
443 ParA$_F$ R320A exhibited mild foci consistent with its slight nucleoid association **(Fig. 8E)**.

444 Our results here show that E375 and R320 are crucial for the polymerisation of $ParA_F$,
445 and mutations in these residues affect the nucleoid localisation and plasmid
446 maintenance function of $ParA_F$. These results further suggest that oligomerisation or
447 formation of higher order structure by $ParA_F$ might be crucial for plasmid partitioning *in*
448 *vivo*.

449 **E375A and R320A mutations affect the super repression activity of $ParA_F$ W362E**

450 We next tested if the introduction of E375A or R320A into $ParA_F$ W362E also
451 abrogated their ability to act as super-repressors of transcription at the P_{parF} promoter
452 site using the above-described LacZ reporter and β-galactosidase assays.
453 Quantification of the β-galactosidase activity in the DLT1127 strain (P_{parA}::*lacZ::kan*)
454 carrying the various $ParA_F$ constructs showed that the double mutants, $ParA_F$ W362E
455 E375A and $ParA_F$ W362E R320A exhibited a decreased ability to repress LacZ
456 expression as compared to $ParA_F$ W362E, indicating that E375A and R320A mutations
457 affected their ability to function as super-repressors **(Fig. 9)**. We used both null
458 hypothesis statistical testing (NHST) and estimation statistics (Claridge-Chang and
459 Assam 2016; Ho et al. 2019) to assess statistical significance of the data. The effect
460 size, defined as the difference in the means, the precision of the difference given by the
461 95 % CI, and p-values for NHST are given in **Table 1 (i – iii)**. While the introduction of
462 R320A into $ParA_F$ W362E led to a difference of -40.1 [-57.8, -22.4] as compared to
463 $ParA_F$ W362E, the effect size in the case of $ParA_F$ W362E E375A was -33.6 [-36.5, -
464 30.8] **(Table 1 i)**.

465 We also assessed the effect of the E375A and R320A single mutations on the
466 repression ability of $ParA_F$. In the absence of the $ParBS_F$ complex, the β-galactosidase
467 activity in the strain carrying $ParA_F$ E375A or $ParA_F$ R320A was not significantly different
468 from those carrying $ParA_F$ **(Table 1 ii)**. However, in the presence of the $ParBS_F$
469 complex, both $ParA_F$ E375A and $ParA_F$ R320A repressed LacZ expression with a
470 difference of 43.4 [30.3, 56.4] and 35.3 [21.5, 49.2], respectively, as compared to the
471 vector control (pDSW210-GFP) **(Table 1 iii)**. On the contrary, $ParA_F$ strongly reduced
472 the expression of LacZ with an effect size of 74 [61.3, 86.7] compared to pDSW210-
473 GFP. Thus, in comparison to $ParA_F$, $ParA_F$ E375A and $ParA_F$ R320A showed a slightly
474 reduced level of repression and had an effect size of -30.7 [-43.7, -17.6] and -38.7 [-
475 52.6, -24.8], respectively **(Table 1 ii)**., showing that $ParA_F$ E375A and $ParA_F$ R320A
476 were moderately defective in repressing the transcriptional activity from the P_{parA}
477 promoter. Nonetheless, $ParA_F$ E375A and $ParA_F$ R320A showed enhanced
478 transcriptional repression in the presence of the $ParBS_F$ complex as compared to its
479 absence, with an effect size of 30.3 [16.0, 44.6] and 24.2 [7.7, 40.6] **(Table 1 iii)**,
480 suggesting that the E375A and R320A mutations did not affect the ParB and nucleotide
481 binding functions of $ParA_F$.

482 **Discussion**

483 DNA partitioning by the ParA family of proteins, such as $ParA_F$ (SopA), depends
484 upon its ability to bind the nucleoid. It is the nucleoid-bound $ParA_F$ that facilitates the
485 process of plasmid segregation by interacting with the ParB-*parC* complex (SopB-
486 *sopC*), which is essentially the plasmid cargo. While initial reports indicated that
487 cytomotive filaments of $ParA_F$ were responsible for the plasmid movements away from

488 the mid-cell (Lim et al. 2005; Leonard et al. 2005; Gitai 2006; Hatano et al. 2007; Bouet
489 et al. 2007), studies from several species of ParA proteins have shown that the ParA
490 proteins interact as ATP-bound dimers with DNA (Vecchiarelli et al. 2010, 2013a; Havey
491 et al. 2012; Lim et al. 2014; Zhang and Schumacher 2017; Köhler et al. 2022; Leonard et
492 al. 2005; Hwang et al. 2013). However, recent studies have suggested that the binding
493 of ParA to the nucleoid is cooperative and a cryo-EM study of $ParA2_{Vc}$ revealed a
494 filament structure of ParA bound to the DNA, suggesting that cooperativity could
495 possibly involve oligomerisation of ParA (Chodha et al. 2023; Köhler et al. 2022; Parker
496 et al. 2021). Thus, the exact function and mechanism of assembly of ParA into higher-
497 order structures remains unclear. Polymerisation of $ParA_F$ has been demonstrated *in*
498 *vitro* (Bouet et al. 2007) in the presence of ATP, and filaments have also been observed
499 in a few cells expressing wild-type $ParA_F$ (Lim et al. 2005; Hatano et al. 2007).

500 A spontaneous mutant of $ParA_F$ (M315I Q351H) has been shown to form static
501 polymeric structures in *E. coli* (Lim et al. 2005). Our studies reported here show that
502 another mutation at position W362 of $ParA_F$ to either E or A also resulted in the
503 assembly of $ParA_F$ into cytoplasmic polymers similar to those formed by $ParA_F$ M315I
504 Q351H (SopA1). Further, a single mutation Q351H was sufficient to stabilise $ParA_F$
505 filaments. Similar assembly of polymers by $ParA_F$ M315I Q351H (SopA1), $ParA_F$
506 Q351H, W362E or the W362A mutants in the absence of the $ParBS_F$ complex or in a
507 heterologous eukaryotic host, fission yeast, suggested that the mutations helped
508 stabilise an otherwise transient polymeric form of $ParA_F$ independent of the partition
509 complex. Moreover, both $ParA_F$ Q351H or $ParA_F$ W362E were able to induce the
510 polymerisation of wild-type $ParA_F$ when co-expressed and resulted in the formation of

511 cytoplasmic filaments of WT-$ParA_F$-GFP, even though $ParA_F$ Q351H exhibited a much
512 stronger effect compared to $ParA_F$ W362E.

513 However, both the mutants (Q351H and W362E), like SopA1 (M315I Q351H),
514 were defective in plasmid maintenance, showing that the static or stable polymers of
515 $ParA_F$ did not drive DNA segregation. Further, super-resolution imaging using 3D-SIM
516 revealed that $ParA_F$ Q351H-GFP and $ParA_F$ W362E-GFP filaments exhibited nucleoid
517 binding defects, consistent with their inability to maintain plasmids. There is ample
518 evidence supporting non-specific DNA binding and dynamic localisation of $ParA_F$ to the
519 nucleoid driving the process of plasmid segregation. These results show that
520 polymerisation in the absence of nucleoid binding does not facilitate plasmid partitioning
521 and maintenance. Moreover, *in vitro* polymerisation studies using light-scattering in the
522 presence of nsDNA have implicated DNA as a polymerisation inhibitor (Bouet et al.
523 2007). Thus, in contrast to Soj and $ParA2_{Vc}$ that form nucleoprotein filaments in the
524 presence of non-specific DNA (Leonard et al. 2005; Hui et al. 2010; Parker et al. 2021),
525 the lack of non-specific DNA binding by $ParA_F$ M315I Q351H (SopA1), $ParA_F$ Q351H
526 and $ParA_F$ W362E could have possibly induced polymerisation. However, K340A, a
527 mutation known to abolish the nsDNA binding in $ParA_F$, does not assemble into such
528 micron-long filaments (Castaing et al. 2008), suggesting that the residues Q351 and
529 W362 in the C-terminal region may play a crucial stabilising role in polymerisation of
530 $ParA_F$.

531 Furthermore, the polymers formed by $ParA_F$ Q351H or $ParA_F$ W362E underwent
532 depolymerisation within 20 minutes when new protein synthesis was stopped,
533 suggesting a need for a critical protein concentration to be maintained in cells for

534 polymerisation. Disassembly of filaments upon inhibition of protein synthesis suggested
535 that the maintenance of the polymers required continual protein synthesis and the
536 existence of a cytoplasmic pool of $ParA_F$ Q351H or $ParA_F$ W362E proteins as well as
537 the polymeric form. Consistent with the inability of $ParA_F$ Q351H or $ParA_F$ W362E
538 proteins to associate with the bacterial nucleoid, both mutations resulted in super-
539 repression of transcription from the $ParA_F$ promoter (P_{parA}), i.e. enhanced transcriptional
540 repression in the absence of the $ParBS_F$ complex. These findings are consistent with
541 the recent reports on $ParA_{P1}$ DNA binding mutants. The absence of nsDNA binding
542 results in an excess-free pool of ParA that becomes available to bind the promoter and
543 function as super-repressors (Baxter et al. 2020). Thus, the inability of $ParA_F$ Q351H
544 and $ParA_F$ W362E to bind nsDNA might create an excess of the free cytoplasmic pool of
545 the protein, which can then exhibit heightened auto-repression activity. We believe that
546 while the filaments may not associate with the nucleoid, the available cytoplasmic pool
547 might interact with the specific $ParA_F$ operator sites, forming a stable complex, acting to
548 prevent transcription effectively. Thus, the mutations (Q351H and W362E) do not impair
549 the ability of $ParA_F$ to bind with specific DNA. These results suggested that the
550 mutations Q351H and W362E did not affect the overall structural integrity of the protein.
551 The mutations Q351H and W362E possibly stabilise the trimer of dimer structures of
552 $ParA_F$ that have been described recently (Boudsocq et al. 2021), enabling the formation
553 of a tighter complex with the $ParA_F$ promoter sites and might be conducive to the
554 organisation of larger filamentous structure beyond a threshold of protein
555 concentrations.

556 Consistent with the earlier *in vitro* studies (Fung et al. 2001; Libante et al. 2001),
557 polymerisation of $ParA_F$ Q351H and W362E was an ATP-dependent process since
558 introducing a mutation that prevents ATP-binding (K120E) completely abolished
559 filament assembly. Mutational studies of the conserved K120 residue in the Walker A
560 motif have also shown that the residue is also crucial for the necessary conformational
561 change from $ParA_F$-ATP to $ParA_F$-ATP* (Libante et al. 2001; Ah-Seng et al. 2013).
562 Accordingly, earlier localisation studies on the various $ParA_F$ K120 substitutions have
563 shown that the K120R and K120Q mutants fail to form foci in the presence of the
564 $ParBS_F$ complex (Hatano et al. 2007). The ability of $ParA_F$ K120A to form foci similar to
565 that of wild-type $ParA_F$ in the presence of the $ParBS_F$ complex suggests that among the
566 various K120 mutants, K120A alone could support the conformational change from
567 $ParA_F$-ATP to $ParA_F$-ATP*. Further, our studies on combining the K120 mutations with
568 W362E show that only $ParA_F$ K120A W362E retained the ability to assemble into
569 filaments. Moreover, previous *in vitro* studies had indicated that $ParA_F$ assembly into
570 filaments possibly depended upon the conformational change induced by ATP. These
571 results suggest that, like nsDNA binding, polymerisation of $ParA_F$ was also dependent
572 upon the conformational change to the $ParA_F$-ATP* state. It is plausible that the
573 mutations Q351H and W362E abolish the ATP hydrolysis activity of $ParA_F$ and stabilise
574 the polymeric state. Interestingly, while the ATP-hydrolysis mutants K120Q or K120A by
575 themselves do not form ParA filaments, yet another mutant, $ParA_F$ V125A, which is also
576 defective in ATP-hydrolysis, has been shown to assemble into polymers *in vivo*
577 (Castaing 2009). Thus, inhibition of ATP-hydrolysis by mutations in the residues other

578 than the conserved K120 in the Walker A motif might result in the stabilisation of $ParA_F$
579 polymers.

580 Clearly, further biochemical experiments on these mutants will be required in the
581 future to address these possibilities and gain insights. On the other hand, we have
582 utilised the ability of $ParA_F$ W362E to form stable filaments to identify new residues
583 crucial for polymerisation for $ParA_F$. Mutations in residues proximal to the previously
584 identified nsDNA binding residues (Castaing et al. 2008) and the C-terminal helix
585 (Mishra et al. 2022) in $ParA_F$ revealed R320 (in helix 14) and E375 in helix 16,
586 respectively, as being critical for the polymerisation of $ParA_F$ W362E. Both $ParA_F$
587 W362E R320A and $ParA_F$ W362E E375A failed to form filaments and exhibited reduced
588 transcriptional repression activity at the $ParA_F$ promoter, suggesting a role for E375 and
589 R320 in oligomerisation/ polymerisation. Accordingly, the single mutants $ParA_F$ R320A
590 and $ParA_F$ E375A also showed reduced promoter repression in the presence of the
591 $ParBS_F$ complex as compared to the WT-$ParA_F$. Nonetheless, both $ParA_F$ R320A and
592 $ParA_F$ E375A responded to ParB and were able to repress the transcriptional activity at
593 the $ParA_F$ promoter in the presence of the $ParBS_F$ partitioning complex, albeit to a
594 lesser extent than wild-type $ParA_F$. Transcriptional repression at the ParA promoter
595 requires nucleotide binding (Lemonnier et al. 2000; Libante et al. 2001; Ah-Seng et al.
596 2013; Baxter et al. 2020). These results, therefore, suggest that the mutations R320A
597 and E375A retained their ability to bind nucleotide and associate with specific promoter
598 DNA sequences to prevent transcription of $ParA_F$ in response to $ParBS_F$. Therefore, we
599 infer that the loss of plasmid maintenance observed for $ParA_F$ R320A and $ParA_F$ E375A
600 was not due to the lack of ATP binding by the mutants but possibly due to their defects

601 in oligomerisation. These results are thus consistent with the recently proposed role of
602 helix 14 and the last C-terminal helix 16 in intra-subunit contacts within $ParA_{Vc}$ filaments
603 (Parker et al., 2021) and co-operative binding of ParA to nsDNA, which may involve
604 polymerisation, albeit transient (Parker et al. 2021; Chodha et al. 2023).

605 We envisage a model wherein upon ATP binding, $ParA_F$ undergoes the
606 conformational change to the $ParA_F$-ATP***** state as proposed earlier and binds co-
607 operatively to nsDNA within the high-density regions (Le Gall et al. 2016; McLeod et al.
608 2017) via assembly into higher-order structures (Hui et al. 2010; Parker et al. 2021).
609 However, the stabilisation of oligomeric structures by the mutants Q351H or W362E
610 results in the formation of long cytoplasmic filaments incompatible with nsDNA binding,
611 resulting in a failure to associate with the nucleoid. Although further biochemical and
612 electron microscopy studies are required to elucidate the oligomerisation of $ParA_F$ and
613 its precise roles *in vivo*, one possibility could be that the polymerisation of $ParA_F$ could
614 act as a sequestration mechanism to regulate any excess $ParA_F$ from the system.
615 Alternately, our studies here lead us to speculate that the last C-terminal helix of $ParA_F$
616 might be a key player in facilitating nsDNA binding and the segregation of plasmids by
617 regulating $ParA_F$ oligomerisation **(Fig. 10)**. Further identification of ParA mutants
618 specifically defective in polymerisation but not in ATP-binding and formation of the ATP-
619 bound sandwich dimers or ParA-ATP* state, and similar studies across other members
620 of the ParA family of DNA partitioning proteins and their genetic and biochemical
621 characterisation should lead to a better insight into the physiological role of
622 polymerisation by the ParA family of proteins.

623

624 ## Materials and Methods

625 ### Strains, Plasmids, Media and Growth Conditions

626 *E. coli* and *S. pombe* strains were cultured as described previously (Srinivasan et
627 al. 2007; Mishra et al. 2021). While *E. coli* was grown at 37°C in LB medium, *S. pombe*
628 was grown at 30°C in Yeast Extract with Supplements (YES) medium or Edinburgh
629 Minimal Medium (EMM) supplemented with adenine (0.225 mg/ml), histidine (0.225
630 mg/ml) and leucine (0.225 mg/ml) or uracil (0.1125 mg/ ml) as necessary but lacking
631 thiamine. Antibiotics carbenicillin and chloramphenicol in LB medium were used at a
632 concentration of 100 µg/ mL and 34 µg/ mL, respectively. Kanamycin was used at 50
633 µg/ mL (for plasmids) or 25 µg/ mL in the case of single-copy chromosomal integrations.
634 Chloramphenicol was added at a 50 µg/ mL concentration to inhibit protein synthesis in
635 cells and at 50 µg/ mL concentration to condense nucleoids (Sun and Margolin 2004;
636 Zusman et al. 1973). Cephalexin at a final concentration of 25 µg/ mL (Pogliano et al.
637 1997) was added to inhibit cell division for 30 minutes. *E. coli* DH5α was used for
638 cloning purposes. All the plasmids used in this study were created using Gibson
639 assembly (Gibson et al. 2009) or Restriction Free cloning (van den Ent and Löwe 2006)
640 and site-directed mutations were introduced by the method of Stratagene
641 QuikChange™ using Q5 polymerase (NEB). In experiments relating to promoter
642 repression, a stop codon (TAA) was introduced between the $ParA_F$ and the GFP coding
643 sequences, as previously reported (Mishra et al. 2022). The strains and plasmids used
644 in this study have been listed in **Supplementary Table S1**, and the oligonucleotides
645 used for generating the constructs have been listed in **Supplementary Table S2**.
646 Expression of $ParA_F$-GFP from the weak P_{Trc} promoter of the pDSW210 vector was

647 achieved by adding 50 μM or 100 μM isopropyl-β-D-thiogalactopyranoside (IPTG) as
648 mentioned in the text.
649
650 **Live Cell Imaging**-
651 Live-cell imaging of *E. coli* and *S. pombe* was carried out as previously described
652 (Srinivasan et al. 2007, 2008; Mishra et al. 2022) using an epifluorescence microscope
653 (DeltaVision Elite^{TM}) equipped with 7-color solid-state illumination (Spectra Light Engine
654 from Lumencor^{TM}). A 100 x oil immersion of NA 1.4 (UPLSAPO100XO) or a phase
655 objective lens (PLN100XOPH) of NA 1.4 was used, and images were acquired using a
656 CCD camera (CoolSNAP^{TM} HQ2). Excitation filters and emission filters of - 390/18 and
657 435/48 (DAPI), 475/28 nm and 525/48 nm (GFP) and 575/25 nm and 625/45 nm
658 (mCherry) were used, respectively. Briefly, cells were pelleted down by centrifuging at
659 2000 x g for 5 min and spotted on LB (for *E. coli*) or EMM without thiamine (for *S.*
660 *pombe*) agarose pads (1.5 % agarose). Nucleoids in *E. coli* were visualised by
661 incubating cells with 0.5 μg/ml 4′,6-diamidino-2-phenylindole (DAPI) for 15–20 min prior
662 to centrifugation. Alternatively, an MG1655-derived strain of *E. coli* expressing HupA-
663 mCherry from its chromosomal locus was used to visualise the nucleoid. Membranes
664 were stained with FM4-64 and additives such as antibiotics, IPTG, 2% glucose,
665 chloramphenicol at 50 ug/ml to prevent protein synthesis or 100 ug/ml to condense
666 nucleoids (Zusman et al. 1973; Sun and Margolin 2004) and cephalexin at 25 μg/ml to
667 prevent cell division (Pogliano et al. 1997) were all added to the agarose pads where
668 mentioned in the text. 3D-SIM imaging was carried out using a DeltaVision OMX-SR
669 Blaze microscope equipped with a PCO Edge 4.2 sCMOS camera, and a 60x, NA 1.42

670 oil-immersion objective lens was used to acquire raw images. An exposure time of 2 – 5
671 ms was used to acquire each image, and Z-stacks were obtained at a step size of 0.125
672 µm to cover the width of the bacterial cell. 3D-SIM images were reconstructed using the
673 SI reconstruction module of SoftWorx™ software. All images were acquired using
674 SoftWorx™ software and processed with Fiji v-1.53c or v-1.54f (Schindelin et al. 2012).
675 The deconvolution of images was performed using SoftWorx™ software's in-built
676 algorithm - DECON3D: 3D iterative constrained deconvolution with not more than 10
677 iterations.
678

679 **Plasmid Stability Assay**

680 Plasmid stability assay was performed using a two-plasmid system (Ah-Seng et
681 al. 2013), as described previously (Mishra et al. 2021, 2022). Briefly, bacterial cultures
682 carrying the plasmids were sub-cultured 1:1000, maintained in exponential phase by
683 sub-culturing (1:100) twice into a fresh LB media and allowed to grow for 40
684 generations. Various dilutions of the culture were plated on carbenicillin plates and
685 incubated at 37 °C. Colonies were then patched on plates containing chloramphenicol
686 to estimate the retention of the mini-F plasmid. The plasmid loss rate was calculated
687 following the equation $L = 100\left[1 - \left(\frac{Ff}{Fi}\right)^{\left[\frac{1}{n}\right]}\right]$ as reported previously (Ravin and Lane
688 1999). “Fi” is the initial fraction of cells containing plasmid, and “Ff” is the number of
689 cells carrying the plasmid after 40 generations (n) of growth.
690

691 **Promoter repression assay**

692 Qualitative assessment to detect the LacZ activity was carried out on LB agar
693 plates containing IPTG (200 μM) and X-gal (40 μg/ mL). Overnight cultures carrying the
694 various $ParA_F$ constructs were diluted 1:100 into fresh LB, and growth was continued
695 until the cultures reached an OD_{600} of 0.2. The cultures were induced with 100 μM IPTG
696 for 2 hours. Subsequently, serial dilutions of the cultures (adjusted to the same OD_{600})
697 were spotted on indicator plates- X-gal (40 μg/ mL) + IPTG (0.2 mM). These plates were
698 then incubated overnight at 37 °C, following which they were imaged using a CCD
699 colour camera on a mobile phone device and the white balance was corrected using the
700 ImageJ plugin. For quantitative estimates of the LacZ expression, β-galactosidase
701 assays were performed as described (Griffith and Wolf 2002). Cultures were centrifuged
702 at 1523 x g, 10 min, 4 °C and the pellet was resuspended in Z-buffer (0.06 M Na_2HPO_4,
703 0.04 M NaH_2PO_4, 0.01 M KCl, 0.001 M $MgSO_4$, pH 7.0). 50 μM β-mercaptoethanol was
704 added to the Z-buffer immediately before use. A 2 mL culture adjusted to an OD_{600} of
705 0.6 was used for all assays. Cells were permeabilised by the addition of 20 μL
706 Chloroform and 20 μL of 0.1 % SDS solution. Samples were then vigorously vortexed
707 for one to 2 minutes and incubated at 28 °C for 10 minutes. Nitrophenyl-β-D-
708 galactopyranoside (ONPG) at a final concentration of 0.13 mM was used as the
709 substrate for the reaction and recorded as time point zero (t_0) for the assay. When
710 ONPG is hydrolysed by β-galactosidase into galactose and *o*-nitrophenol, the solution
711 colour turns yellow. When sufficient yellow colour had developed (assessed visually),
712 the reaction was stopped by the addition of 100 μL of 1 M solution of Na_2CO_3 and the
713 time was recorded (in minutes). Values of the β- galactosidase activity were determined
714 in Miller units using the formula: $MU = 1000 \times \left[\frac{\{OD_{420}-(1.75\times OD_{550})\}}{T\times V\times OD_{600}}\right]$, where MU is Miller

715 Units, OD_{420}, OD_{550} and OD_{600} are measure optical density at 420 nm, 550 nm and 600
716 nm, respectively. T is the total reaction time in minutes, and V is the volume of culture
717 used in milli-litres (mL).
718
719 **Statistical Methods**
720 A single colony of bacteria or a patch of yeast cells from freshly streaked out cells on
721 agar plates from frozen glycerol stocks and grown independently were considered biological
722 replicates (n). Except where mentioned in the text, every experiment was performed at
723 least 3 or more times (independent biological replicates, $n \geq 3$). All error bars represent
724 the standard deviation from the central tendency value mean. In the case of the plasmid
725 stability assays, the loss rate of mini-F plasmid was compared to the cultures that
726 carried the wild-type $ParA_F$, wherein the plasmid loss rate was always zero. Therefore, a
727 one-sample t-test was used to calculate p-values for evaluating the statistical
728 significance of the plasmid loss rates among various mutants. The online web server
729 https://www.graphpad.com/quickcalcs/oneSampleT1/ was used to obtain the p-values.
730 For other experiments pertaining to the promoter repression assays, where p-values are
731 mentioned, either two-tailed Student's t-test or one-tailed Student's t-test was used,
732 wherein the repression values were already expected to be only higher, as in the case
733 of vector control (normalised to zero) and ParBS (which is expected to enhance
734 repression). As an alternative to null-hypothesis significance tests (NHST), we also
735 used estimation statistics to determine the effect size and the precision of the effect size
736 was given by the 95 % confidence intervals (Claridge-Chang and Assam 2016; Ho et al.
737 2019). Superplots were plotted as described (Lord et al. 2020) using Excel Office 365.
738 Effect size is defined as the difference between the mean values of the samples being

compared, and statistical significance is assumed when 95% CI values do not encompass zero (Cumming et al. 2007; Vaux 2014; Pollard et al. 2019).

Acknowledgement

The authors thank all the members of the RS lab for their helpful suggestions and technical help. DM and NM received financial support and fellowship from DAE, which is acknowledged. RS is the recipient of research grants from DST-SERB (CRG/2021/000337) that supported this work. Intra-mural funding from the Department of Atomic Energy (DAE) is acknowledged. The authors sincerely thank Drs. Anjana Badrinarayanan (NCBS, TIFR, DAE) and Gayathri Pananghat for their suggestions, helpful discussions and comments on the manuscript. The authors thank Drs. Jean Yves-Bouet (LMGM, Toulouse, France), David Lane (CBI-Toulouse, France), Tushar Beuria (ILS, Bhubaneswar) and Mohan Chandra Joshi (JMI, New Delhi), for the generous gifts of strains and plasmid. pDSW210 was originally a gift from Dr. David Weiss (Univ. of Iowa), and the *E. coli ΔminB* strain was originally obtained from Dr. Lutkenhaus (Univ. of Kansas).

Author Contributions

NM, DM and IAP performed experiments. NM and DM carried out microscopy, acquired images and analysed them. IAP performed and analysed certain experiments pertaining to promoter repression and analysed images. NM quantified, analysed and organised the data. NM and DM contributed to writing the draft manuscript. RS and NM edited the

761 manuscript. RS conceptualised the work, RS and NM designed experiments, analysed
762 and interpreted the data.
763
764 **References:**
765

766 Abeles AL, Friedman SA, Austin SJ. 1985. Partition of unit-copy miniplasmids to
767 daughter cells. *J Mol Biol* **185**: 261–272.

768 Ah-Seng Y, Lopez F, Pasta F, Lane D, Bouet J-Y. 2009. Dual role of DNA in regulating
769 ATP hydrolysis by the SopA partition protein. *J Biol Chem* **284**: 30067–30075.

770 Ah-Seng Y, Rech J, Lane D, Bouet J-Y. 2013. Defining the role of ATP hydrolysis in
771 mitotic segregation of bacterial plasmids. *PLoS Genet* **9**: e1003956.

772 Anand SP, Akhtar P, Tinsley E, Watkins SC, Khan SA. 2008. GTP-dependent
773 polymerization of the tubulin-like RepX replication protein encoded by the pXO1
774 plasmid of Bacillus anthracis. *Mol Microbiol* **67**: 881–890.

775 Barillà D, Carmelo E, Hayes F. 2007. The tail of the ParG DNA segregation protein
776 remodels ParF polymers and enhances ATP hydrolysis via an arginine finger-like
777 motif. *Proc Natl Acad Sci USA* **104**: 1811–1816.

778 Barillà D, Rosenberg MF, Nobbmann U, Hayes F. 2005. Bacterial DNA segregation
779 dynamics mediated by the polymerizing protein ParF. *EMBO J* **24**: 1453–1464.

780 Basi G, Schmid E, Maundrell K. 1993. TATA box mutations in the
781 Schizosaccharomyces pombe nmt1 promoter affect transcription efficiency but not the
782 transcription start point or thiamine repressibility. *Gene* **123**: 131–136.

783 Baxter JC, Waples WG, Funnell BE. 2020. Nonspecific DNA binding by P1 ParA
784 determines the distribution of plasmid partition and repressor activities. *J Biol Chem*
785 **295**: 17298–17309.

786 Boudsocq F, Salhi M, Barbe S, Bouet J-Y. 2021. Three para dimers cooperatively
787 assemble on type ia partition promoters. *Genes* **12**.

788 Bouet J-Y, Ah-Seng Y, Benmeradi N, Lane D. 2007. Polymerization of SopA partition
789 ATPase: regulation by DNA binding and SopB. *Mol Microbiol* **63**: 468–481.

790 Brooks AC, Hwang LC. 2017. Reconstitutions of plasmid partition systems and their
791 mechanisms. *Plasmid* **91**: 37–41.

792 Caccamo M, Dobruk-Serkowska A, Rodríguez-Castañeda F, Pennica C, Barillà D,
793 Hayes F. 2020. Genome segregation by the venus flytrap mechanism: probing the
794 interaction between the ParF ATPase and the parG centromere binding protein. *Front*
795 *Mol Biosci* **7**: 108.

796 Castaing J-P, Bouet J-Y, Lane D. 2008. F plasmid partition depends on interaction of
797 SopA with non-specific DNA. *Mol Microbiol* **70**: 1000–1011.

798 Castaing J-P. 2009. La ségrégation du plasmide F d'*Escherichia coli* : Étude du rôle de
799 la fixation de l'ATPase SopA à l'ADN. Doctoral dissertation.

800 Cerceo E, Deitelzweig SB, Sherman BM, Amin AN. 2016. Multidrug-Resistant Gram-
801 Negative Bacterial Infections in the Hospital Setting: Overview, Implications for
802 Clinical Practice, and Emerging Treatment Options. *Microb Drug Resist* **22**: 412–431.

803 Chodha SS, Brooks AC, Davis PJ, Ramachandran R, Chattoraj DK, Hwang LC. 2023.
804 Kinetic principles of ParA2-ATP cycling guide dynamic subcellular localizations in
805 Vibrio cholerae. *Nucleic Acids Res* **51**: 5603–5620.

806 Claridge-Chang A, Assam PN. 2016. Estimation statistics should replace significance
807 testing. *Nat Methods* **13**: 108–109.

808 Cumming G, Fidler F, Vaux DL. 2007. Error bars in experimental biology. *J Cell Biol*
809 **177**: 7–11.

810 Davis MA, Radnedge L, Martin KA, Hayes F, Youngren B, Austin SJ. 1996. The P1
811 ParA protein and its ATPase activity play a direct role in the segregation of plasmid
812 copies to daughter cells. *Mol Microbiol* **21**: 1029–1036.

813 Dobruk-Serkowska A, Caccamo M, Rodríguez-Castañeda F, Wu M, Bryce K, Ng I,
814 Schumacher MA, Barillà D, Hayes F. 2012. Uncoupling of nucleotide hydrolysis and
815 polymerization in the ParA protein superfamily disrupts DNA segregation dynamics. *J*
816 *Biol Chem* **287**: 42545–42553.

817 Ebersbach G, Gerdes K. 2001. The double par locus of virulence factor pB171: DNA
818 segregation is correlated with oscillation of ParA. *Proc Natl Acad Sci USA* **98**: 15078–
819 15083.

820 Fung E, Bouet JY, Funnell BE. 2001. Probing the ATP-binding site of P1 ParA: partition
821 and repression have different requirements for ATP binding and hydrolysis. *EMBO J*
822 **20**: 4901–4911.

823 Gibson DG, Young L, Chuang R-Y, Venter JC, Hutchison CA, Smith HO. 2009.
824 Enzymatic assembly of DNA molecules up to several hundred kilobases. *Nat Methods*
825 **6**: 343–345.

826 Gitai Z. 2006. Plasmid segregation: a new class of cytoskeletal proteins emerges. *Curr*
827 *Biol* **16**: R133-6.

828 Griffith KL, Wolf RE. 2002. Measuring beta-galactosidase activity in bacteria: cell
829 growth, permeabilization, and enzyme assays in 96-well arrays. *Biochem Biophys*
830 *Res Commun* **290**: 397–402.

831 Hatano T, Niki H. 2010. Partitioning of P1 plasmids by gradual distribution of the
832 ATPase ParA. *Mol Microbiol* **78**: 1182–1198.

833 Hatano T, Yamaichi Y, Niki H. 2007. Oscillating focus of SopA associated with
834 filamentous structure guides partitioning of F plasmid. *Mol Microbiol* **64**: 1198–1213.

835 Havey JC, Vecchiarelli AG, Funnell BE. 2012. ATP-regulated interactions between P1
836 ParA, ParB and non-specific DNA that are stabilized by the plasmid partition site,
837 parS. *Nucleic Acids Res* **40**: 801–812.

838 Hayes F, Radnedge L, Davis MA, Austin SJ. 1994. The homologous operons for P1 and
839 P7 plasmid partition are autoregulated from dissimilar operator sites. *Mol Microbiol* **11**:
840 249–260.

841 Hirano M, Mori H, Onogi T, Yamazoe M, Niki H, Ogura T, Hiraga S. 1998.
842 Autoregulation of the partition genes of the mini-F plasmid and the intracellular
843 localization of their products in Escherichia coli. *Mol Gen Genet* **257**: 392–403.

844 Ho J, Tumkaya T, Aryal S, Choi H, Claridge-Chang A. 2019. Moving beyond P values:
845 data analysis with estimation graphics. *Nat Methods* **16**: 565–566.

846 Hui MP, Galkin VE, Yu X, Stasiak AZ, Stasiak A, Waldor MK, Egelman EH. 2010.
847 ParA2, a Vibrio cholerae chromosome partitioning protein, forms left-handed helical
848 filaments on DNA. *Proc Natl Acad Sci USA* **107**: 4590–4595.

849 Hu L, Rech J, Bouet J-Y, Liu J. 2021. Spatial control over near-critical-point operation
850 ensures fidelity of ParABS-mediated DNA partition. *Biophys J* **120**: 3911–3924.

851 Hu L, Vecchiarelli AG, Mizuuchi K, Neuman KC, Liu J. 2017. Brownian Ratchet
852 Mechanism for Faithful Segregation of Low-Copy-Number Plasmids. *Biophys J* **112**:
853 1489–1502.

854 Hu L, Vecchiarelli AG, Mizuuchi K, Neuman KC, Liu J. 2015. Directed and persistent
855 movement arises from mechanochemistry of the ParA/ParB system. *Proc Natl Acad*
856 *Sci USA* **112**: E7055-64.

857 Hwang LC, Vecchiarelli AG, Han Y-W, Mizuuchi M, Harada Y, Funnell BE, Mizuuchi K.
858 2013. ParA-mediated plasmid partition driven by protein pattern self-organization.
859 *EMBO J* **32**: 1238–1249.

860 Jalil MB, Al Atbee MYN. 2022. The prevalence of multiple drug resistance Escherichia
861 coli and Klebsiella pneumoniae isolated from patients with urinary tract infections. *J*
862 *Clin Lab Anal* **36**: e24619.

863 Köhler R, Kaganovitch E, Murray SM. 2022. High-throughput imaging and quantitative
864 analysis uncovers the nature of plasmid positioning by ParABS. *eLife* **11**.

865 Komai M, Umino M, Hanai R. 2011. Mode of DNA binding by SopA protein of
866 Escherichia coli F plasmid. *J Biochem* **149**: 455–461.

867 Koonin EV. 1993. A superfamily of ATPases with diverse functions containing either
868 classical or deviant ATP-binding motif. *J Mol Biol* **229**: 1165–1174.

869 Lane D, Rothenbuehler R, Merrillat AM, Aiken C. 1987. Analysis of the F plasmid
870 centromere. *Mol Gen Genet* **207**: 406–412.

871 Larsen RA, Cusumano C, Fujioka A, Lim-Fong G, Patterson P, Pogliano J. 2007.
872 Treadmilling of a prokaryotic tubulin-like protein, TubZ, required for plasmid stability in
873 Bacillus thuringiensis. *Genes Dev* **21**: 1340–1352.

874 Le Gall A, Cattoni DI, Guilhas B, Mathieu-Demazière C, Oudjedi L, Fiche J-B, Rech J,
875 Abrahamsson S, Murray H, Bouet J-Y, et al. 2016. Bacterial partition complexes
876 segregate within the volume of the nucleoid. *Nat Commun* **7**: 12107.

877 Lee PS, Grossman AD. 2006. The chromosome partitioning proteins Soj (ParA) and
878 Spo0J (ParB) contribute to accurate chromosome partitioning, separation of replicated
879 sister origins, and regulation of replication initiation in Bacillus subtilis. *Mol Microbiol*
880 **60**: 853–869.

881 Lemonnier M, Bouet JY, Libante V, Lane D. 2000. Disruption of the F plasmid partition
882 complex in vivo by partition protein SopA. *Mol Microbiol* **38**: 493–505.

883 Leonard TA, Butler PJ, Löwe J. 2005. Bacterial chromosome segregation: structure and
884 DNA binding of the Soj dimer--a conserved biological switch. *EMBO J* **24**: 270–282.

885 Leonard TA, Butler PJG, Löwe J. 2004. Structural analysis of the chromosome
886 segregation protein Spo0J from Thermus thermophilus. *Mol Microbiol* **53**: 419–432.

887 Libante V, Thion L, Lane D. 2001. Role of the ATP-binding site of SopA protein in
888 partition of the F plasmid. *J Mol Biol* **314**: 387–399.

889 Lim GE, Derman AI, Pogliano J. 2005. Bacterial DNA segregation by dynamic SopA
890 polymers. *Proc Natl Acad Sci USA* **102**: 17658–17663.

891 Lim HC, Surovtsev IV, Beltran BG, Huang F, Bewersdorf J, Jacobs-Wagner C. 2014.
892 Evidence for a DNA-relay mechanism in ParABS-mediated chromosome segregation.
893 *eLife* **3**: e02758.

894 Lord SJ, Velle KB, Mullins RD, Fritz-Laylin LK. 2020. SuperPlots: Communicating
895 reproducibility and variability in cell biology. *J Cell Biol* **219**.

896 Lutkenhaus J. 2012. The ParA/MinD family puts things in their place. *Trends Microbiol*
897 **20**: 411–418.

898 Machado E, Costa P, Carvalho A, On Behalf Of The Sarel Investigators. 2022.
899 Occurrence of Healthcare-Associated Infections (HAIs) by Escherichia coli and
900 Klebsiella spp. Producing Extended-Spectrum β-lactamases (ESBL) and/or
901 Carbapenemases in Portuguese Long-Term Care Facilities. *Pathogens* **11**.

902 McLeod BN, Allison-Gamble GE, Barge MT, Tonthat NK, Schumacher MA, Hayes F,
903 Barillà D. 2017. A three-dimensional ParF meshwork assembles through the nucleoid
904 to mediate plasmid segregation. *Nucleic Acids Res* **45**: 3158–3171.

905 Meynell E, Meynell GG, Datta N. 1968. Phylogenetic relationships of drug-resistance
906 factors and other transmissible bacterial plasmids. *Bacteriol Rev* **32**: 55–83.

907 Mishra D, Jakhmola A, Srinivasan R. 2022. A role for the last C-terminal helix of the F
908 plasmid segregating protein SopA in nucleoid binding and plasmid maintenance.
909 *Plasmid* **119–120**: 102617.

910 Mishra D, Pahujani S, Mitra N, Srivastava A, Srinivasan R. 2021. Identification of a
911 Potential Membrane-Targeting Sequence in the C-Terminus of the F Plasmid
912 Segregation Protein SopA. *J Membr Biol* **254**: 243–257.

913 Møller-Jensen J, Borch J, Dam M, Jensen RB, Roepstorff P, Gerdes K. 2003. Bacterial
914 mitosis: ParM of plasmid R1 moves plasmid DNA by an actin-like insertional
915 polymerization mechanism. *Mol Cell* **12**: 1477–1487.

916 Moran RA, Anantham S, Pinyon JL, Hall RM. 2015. Plasmids in antibiotic susceptible
917 and antibiotic resistant commensal Escherichia coli from healthy Australian adults.
918 *Plasmid* **80**: 24–31.

919 Mori H, Mori Y, Ichinose C, Niki H, Ogura T, Kato A, Hiraga S. 1989. Purification and
920 characterization of SopA and SopB proteins essential for F plasmid partitioning. *J Biol*
921 *Chem* **264**: 15535–15541.

922 Motallebi-Veshareh M, Rouch DA, Thomas CM. 1990. A family of ATPases involved in
923 active partitioning of diverse bacterial plasmids. *Mol Microbiol* **4**: 1455–1463.

924 Niki H, Hiraga S. 1997. Subcellular distribution of actively partitioning F plasmid during
925 the cell division cycle in E. coli. *Cell* **90**: 951–957.

926 Ogura T, Hiraga S. 1983. Partition mechanism of F plasmid: two plasmid gene-encoded
927 products and a cis-acting region are involved in partition. *Cell* **32**: 351–360.

928 Pande V, Mitra N, Bagde SR, Srinivasan R, Gayathri P. 2022. Filament organization of
929 the bacterial actin MreB is dependent on the nucleotide state. *J Cell Biol* **221**.

930 Parker AV, Mann D, Tzokov SB, Hwang LC, Bergeron JRC. 2021. The structure of the
931 bacterial DNA segregation ATPase filament reveals the conformational plasticity of
932 ParA upon DNA binding. *Nat Commun* **12**: 5166.

933 Phan MD, Forde BM, Peters KM, Sarkar S, Hancock S, Stanton-Cook M, Ben Zakour
934 NL, Upton M, Beatson SA, Schembri MA. 2015. Molecular characterization of a

935 multidrug resistance IncF plasmid from the globally disseminated Escherichia coli
936 ST131 clone. *PLoS ONE* **10**: e0122369.

937 Pogliano J, Pogliano K, Weiss DS, Losick R, Beckwith J. 1997. Inactivation of FtsI
938 inhibits constriction of the FtsZ cytokinetic ring and delays the assembly of FtsZ rings
939 at potential division sites. *Proc Natl Acad Sci USA* **94**: 559–564.

940 Pollard DA, Pollard TD, Pollard KS. 2019. Empowering statistical methods for cellular
941 and molecular biologists. *Mol Biol Cell* **30**: 1359–1368.

942 Ravin N, Lane D. 1999. Partition of the linear plasmid N15: interactions of N15 partition
943 functions with the sop locus of the F plasmid. *J Bacteriol* **181**: 6898–6906.

944 Ravin NV, Rech J, Lane D. 2003. Mapping of functional domains in F plasmid partition
945 proteins reveals a bipartite SopB-recognition domain in SopA. *J Mol Biol* **329**: 875–
946 889.

947 Ringgaard S, van Zon J, Howard M, Gerdes K. 2009. Movement and equipositioning of
948 plasmids by ParA filament disassembly. *Proc Natl Acad Sci USA* **106**: 19369–19374.

949 Roberts MAJ, Wadhams GH, Hadfield KA, Tickner S, Armitage JP. 2012. ParA-like
950 protein uses nonspecific chromosomal DNA binding to partition protein complexes.
951 *Proc Natl Acad Sci USA* **109**: 6698–6703.

952 Salje J, Gayathri P, Löwe J. 2010. The ParMRC system: molecular mechanisms of
953 plasmid segregation by actin-like filaments. *Nat Rev Microbiol* **8**: 683–692.

954 Schindelin J, Arganda-Carreras I, Frise E, Kaynig V, Longair M, Pietzsch T, Preibisch S,
955 Rueden C, Saalfeld S, Schmid B, et al. 2012. Fiji: an open-source platform for
956 biological-image analysis. *Nat Methods* **9**: 676–682.

957 Schumacher MA, Ye Q, Barge MT, Zampini M, Barillà D, Hayes F. 2012. Structural
958 mechanism of ATP-induced polymerization of the partition factor ParF: implications for
959 DNA segregation. *J Biol Chem* **287**: 26146–26154.

960 Simonsen GS. 2018. Antimicrobial resistance surveillance in Europe and beyond. *Euro*
961 *Surveill* **23**.

962 Srinivasan R, Mishra M, Murata-Hori M, Balasubramanian MK. 2007. Filament
963 formation of the Escherichia coli actin-related protein, MreB, in fission yeast. *Curr Biol*
964 **17**: 266–272.

965 Srinivasan R, Mishra M, Wu L, Yin Z, Balasubramanian MK. 2008. The bacterial cell
966 division protein FtsZ assembles into cytoplasmic rings in fission yeast. *Genes Dev* **22**:
967 1741–1746.

968 Stephens C, Arismendi T, Wright M, Hartman A, Gonzalez A, Gill M, Pandori M, Hess
969 D. 2020. F Plasmids Are the Major Carriers of Antibiotic Resistance Genes in Human-
970 Associated Commensal Escherichia coli. *mSphere* **5**.

971 Sun Q, Margolin W. 2004. Effects of perturbing nucleoid structure on nucleoid
972 occlusion-mediated toporegulation of FtsZ ring assembly. *J Bacteriol* **186**: 3951–3959.

973 Surovtsev IV, Campos M, Jacobs-Wagner C. 2016. DNA-relay mechanism is sufficient
974 to explain ParA-dependent intracellular transport and patterning of single and multiple
975 cargos. *Proc Natl Acad Sci USA* **113**: E7268–E7276.

976 TerBush AD, MacCready JS, Chen C, Ducat DC, Osteryoung KW. 2018. Conserved
977 dynamics of chloroplast cytoskeletal ftsz proteins across photosynthetic lineages.
978 *Plant Physiol* **176**: 295–306.

979 TerBush AD, Osteryoung KW. 2012. Distinct functions of chloroplast FtsZ1 and FtsZ2 in
980 Z-ring structure and remodeling. *J Cell Biol* **199**: 623–637.

981 Tinsley E, Khan SA. 2006. A novel FtsZ-like protein is involved in replication of the
982 anthrax toxin-encoding pXO1 plasmid in Bacillus anthracis. *J Bacteriol* **188**: 2829–
983 2835.

984 van den Ent F, Löwe J. 2006. RF cloning: a restriction-free method for inserting target
985 genes into plasmids. *J Biochem Biophys Methods* **67**: 67–74.

986 van den Ent F, Møller-Jensen J, Amos LA, Gerdes K, Löwe J. 2002. F-actin-like
987 filaments formed by plasmid segregation protein ParM. *EMBO J* **21**: 6935–6943.

988 Vaux DL. 2014. Basic statistics in cell biology. *Annu Rev Cell Dev Biol* **30**: 23–37.

989 Vecchiarelli AG, Han Y-W, Tan X, Mizuuchi M, Ghirlando R, Biertümpfel C, Funnell BE,
990 Mizuuchi K. 2010. ATP control of dynamic P1 ParA-DNA interactions: a key role for
991 the nucleoid in plasmid partition. *Mol Microbiol* **78**: 78–91.

992 Vecchiarelli AG, Havey JC, Ing LL, Wong EOY, Waples WG, Funnell BE. 2013a.
993 Dissection of the ATPase active site of P1 ParA reveals multiple active forms
994 essential for plasmid partition. *J Biol Chem* **288**: 17823–17831.

995 Vecchiarelli AG, Hwang LC, Mizuuchi K. 2013b. Cell-free study of F plasmid partition
996 provides evidence for cargo transport by a diffusion-ratchet mechanism. *Proc Natl*
997 *Acad Sci USA* **110**: E1390-7.

998 Vecchiarelli AG, Mizuuchi K, Funnell BE. 2012. Surfing biological surfaces: exploiting
999 the nucleoid for partition and transport in bacteria. *Mol Microbiol* **86**: 513–523.

1000 Vecchiarelli AG, Neuman KC, Mizuuchi K. 2014. A propagating ATPase gradient drives
1001 transport of surface-confined cellular cargo. *Proc Natl Acad Sci USA* **111**: 4880–4885.

1002 Volante A, Alonso JC. 2015. Molecular Anatomy of ParA-ParA and ParA-ParB
1003 Interactions during Plasmid Partitioning. *J Biol Chem* **290**: 18782–18795.

1004 Walker JE, Saraste M, Runswick MJ, Gay NJ. 1982. Distantly related sequences in the
1005 alpha- and beta-subunits of ATP synthase, myosin, kinases and other ATP-requiring
1006 enzymes and a common nucleotide binding fold. *EMBO J* **1**: 945–951.

1007 Watanabe E, Wachi M, Yamasaki M, Nagai K. 1992. ATPase activity of SopA, a protein
1008 essential for active partitioning of F plasmid. *Mol Gen Genet* **234**: 346–352.

1009 World Health Organization (GLASS). 2021. *Global Antimicrobial Resistance and Use*
1010 *Surveillance System (GLASS) Report: 2021*. World Health Organization
1011 https://www.who.int/publications/i/item/9789240027336 (Accessed June 12, 2022).

1012 Yates P, Lane D, Biek DP. 1999. The F plasmid centromere, sopC, is required for full
1013 repression of the sopAB operon. *J Mol Biol* **290**: 627–638.

1014 Yong D, Toleman MA, Giske CG, Cho HS, Sundman K, Lee K, Walsh TR. 2009.
1015 Characterization of a new metallo-beta-lactamase gene, bla(NDM-1), and a novel
1016 erythromycin esterase gene carried on a unique genetic structure in Klebsiella
1017 pneumoniae sequence type 14 from India. *Antimicrob Agents Chemother* **53**: 5046–
1018 5054.

1019 Zhang H, Schumacher MA. 2017. Structures of partition protein ParA with nonspecific
1020 DNA and ParB effector reveal molecular insights into principles governing Walker-box
1021 DNA segregation. *Genes Dev* **31**: 481–492.

1022 Zusman DR, Carbonell A, Haga JY. 1973. Nucleoid condensation and cell division in
1023 Escherichia coli MX74T2 ts52 after inhibition of protein synthesis. *J Bacteriol* **115**:
1024 1167–1178.
1025

1026

1027

1028 # Figures, Figure Legends and Tables

Figure 1

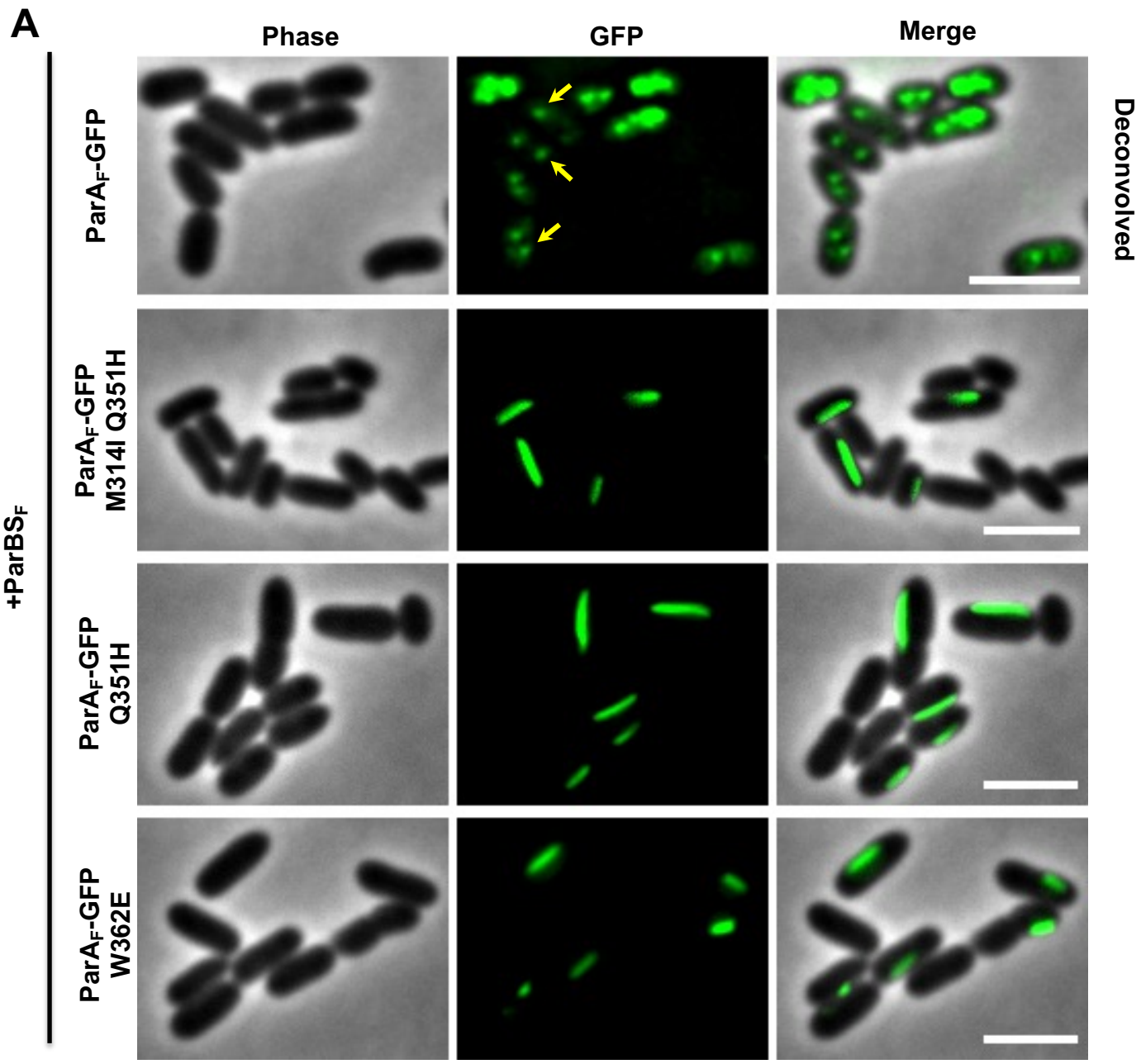
A
Phase
GFP
Merge
Deconvolved
+ParBS$_F$
ParA$_F$-GFP
ParA$_F$-GFP M314I Q351H
ParA$_F$-GFP Q351H
ParA$_F$-GFP W362E

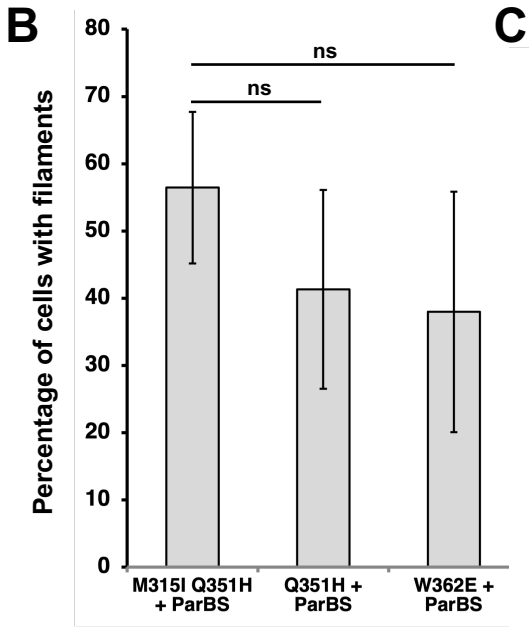
B
Percentage of cells with filaments
80
70
60
50
40
30
20
10
0
ns
ns
M315I Q351H + ParBS
Q351H + ParBS
W362E + ParBS

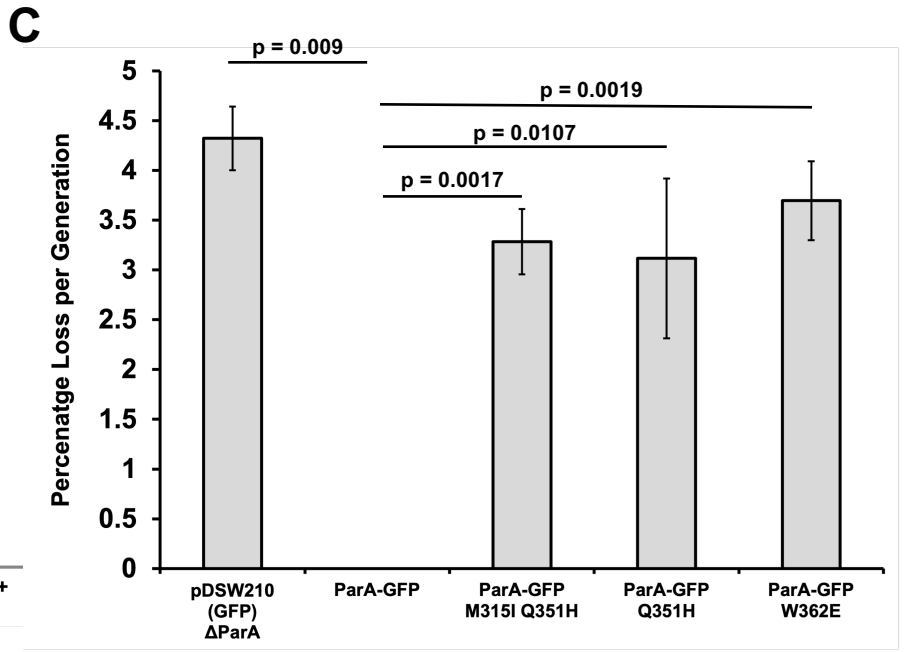
C
Percenatge Loss per Generation
5
4.5
4
3.5
3
2.5
2
1.5
1
0.5
0
p = 0.009
p = 0.0019
p = 0.0107
p = 0.0017
pDSW210 (GFP) ΔParA
ParA-GFP
ParA-GFP M315I Q351H
ParA-GFP Q351H
ParA-GFP W362E

Figure 1. $ParA_F$ Q351H and $ParA_F$ W362E assemble into cytoplasmic filaments in *E. coli*.

(A) In the presence of the ParBS complex, wild-type $ParA_F$-GFP appears as a haze or forms foci. $ParA_F$ M315I Q351H-GFP (SopA1-GFP), $ParA_F$ Q351H-GFP and $ParA_F$ W362E assemble into linear cytoplasmic filaments. $ParA_F$ and the various mutants described were expressed from the weak P_{trc} promoter in pDSW210 as C-terminal GFP fusions by the addition of 100 μM IPTG for 2 hours in *E. coli* MC4100. Cultures were grown to an OD_{600} of 0.2 before the addition of IPTG for protein expression. A mini-F plasmid carried the *parBS* locus under the constitutive P_{LtetO} promoter and lacked $ParA_F$ (*Δ*$parA_F$ *parBS*$^+$). **(B)** Quantification of percentage of cells carrying $ParA_F$ M315I Q351H-GFP (SopA1-GFP), $ParA_F$ Q351H-GFP and $ParA_F$ W362E-GFP filaments. Percentage of cells having filaments were 56.5 % ± 11.27, 41.3 % ± 14.8 and 38.0 % ± 17.9 (95% CI, n=3; number of cells counted > 100 for each experiment) in the case of $ParA_F$ M315I Q351H-GFP, $ParA_F$ Q351H-GFP and $ParA_F$ W362E-GFP, respectively. **(C)** Quantification of loss of the mini-F plasmids in cultures carrying wild-type $ParA_F$-GFP, $ParA_F$ M315I Q351H-GFP (SopA1-GFP), $ParA_F$ Q351H-GFP and $ParA_F$ W362E-GFP. While $ParA_F$-GFP maintained the plasmids stably, the loss of plasmids in all $ParA_F$ mutants was similar to that of the vector control (lacking $ParA_F$ but expressing GFP alone). The partitioning complex ParBS (where indicated) was provided from a mini-F plasmid (pDAG198; *Δ*$parA_F$ *parBS*$^+$) that lacked $ParA_F$ but carried the *parBS* locus under the constitutive P_{LtetO} promoter. The same two plasmids were used for the plasmid stability assays in **(A)**. Cells were mounted onto a 1.6% LB agarose slide and imaged using an epifluorescence microscope. A two-sided Student's -t-test was used to calculate P-values in case of **(B)**,

and since we expect the plasmid loss in $ParA_F$ mutants to be only higher than in $ParA_F$, a one-sided one-sample t-test was used to assess the significance in this case **(C)**. ns represents a p-value > 0.05. All experiments were repeated at least thrice (n = 3, three biological replicates). Error bars in **(B)** are inferential and represent the 95% confidence interval and the error bars in **(C)** represent the standard deviation (SD) of the mean. Scale bars represent 3 μm for all images.

Figure 2

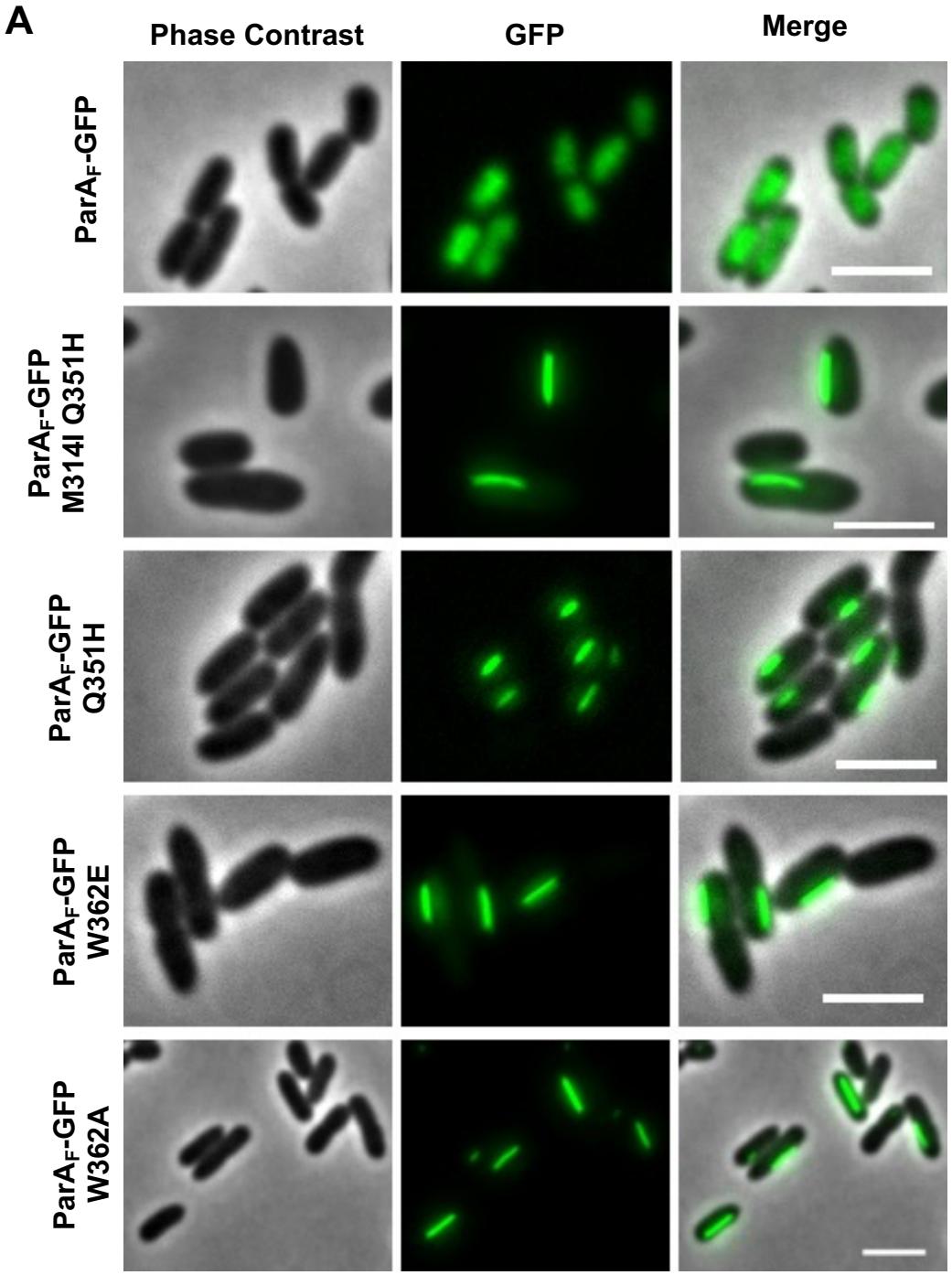
A
Phase Contrast
GFP
Merge
ParAF-GFP
ParAF-GFP M314I Q351H
ParAF-GFP Q351H
ParAF-GFP W362E
ParAF-GFP W362A

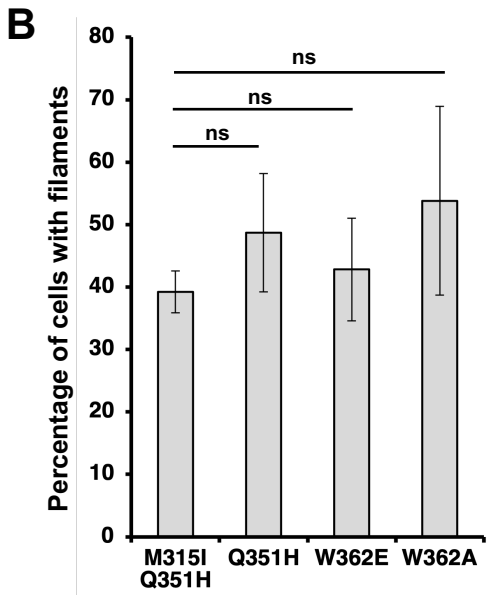
B
Percentage of cells with filaments
0
10
20
30
40
50
60
70
80
ns
ns
ns
M315I Q351H
Q351H
W362E
W362A

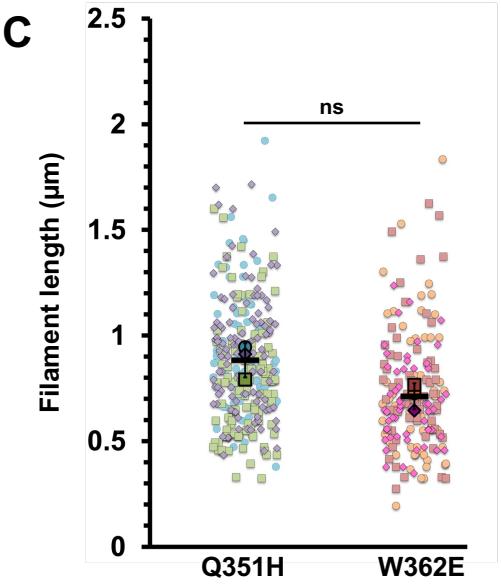
C
Filament length (µm)
0
0.5
1
1.5
2
2.5
ns
Q351H
W362E

Figure 2

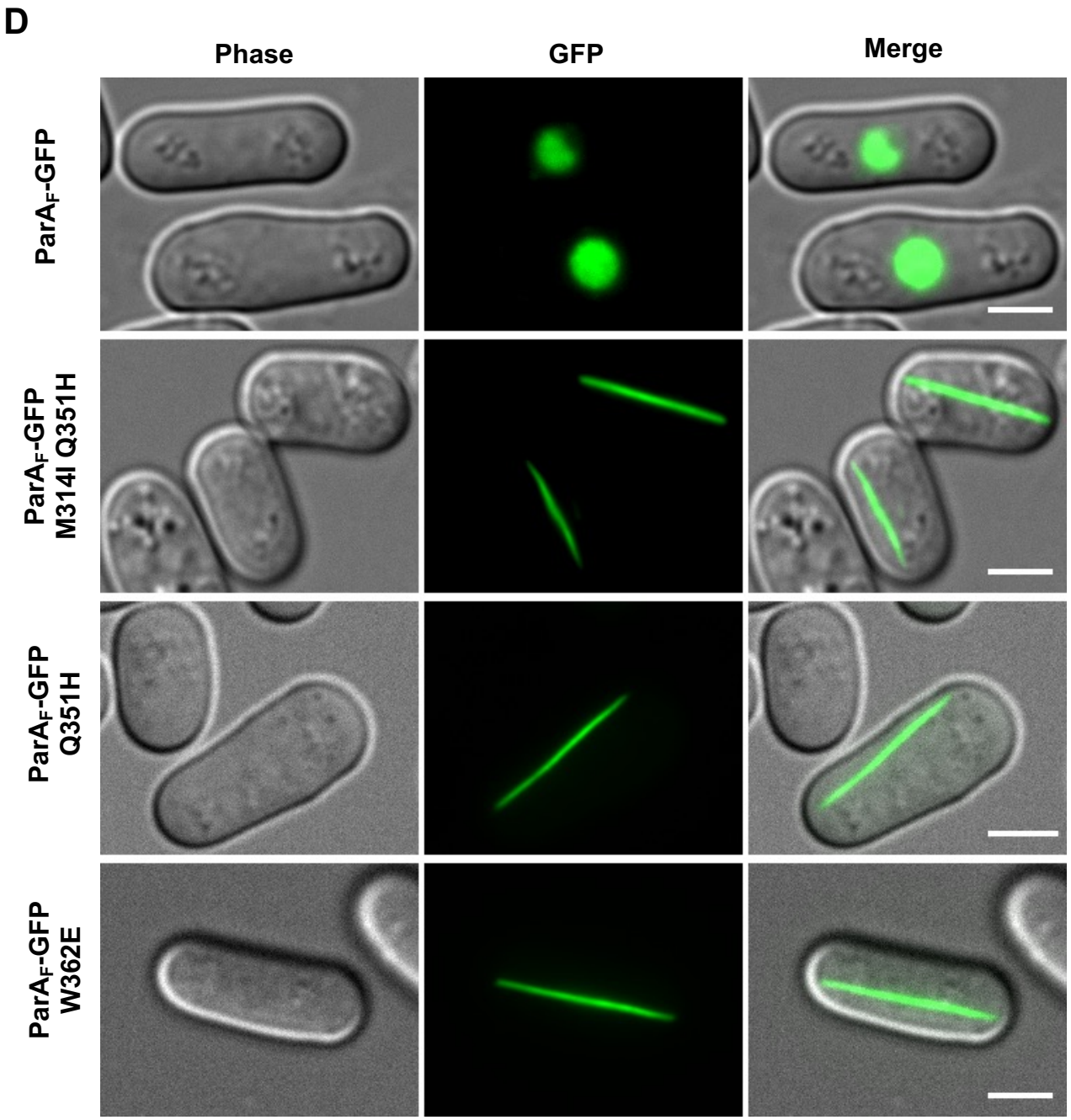
D
Phase
GFP
Merge
ParAF-GFP
ParAF-GFP M314I Q351H
ParAF-GFP Q351H
ParAF-GFP W362E

Figure 2. Assembly of $ParA_F$ Q351H, $ParA_F$ W362E or $ParA_F$ W362A into cytoplasmic filaments is independent of the *parBS* partitioning complex.

(A) In the absence of the *parBS* complex, $ParA_F$-GFP does not form foci but appears to be over the nucleoid. $ParA_F$ M315I Q351H-GFP (SopA1-GFP), $ParA_F$ Q351H-GFP, $ParA_F$ W362E-GFP and $ParA_F$ W362A-GFP assemble into straight cytoplasmic filaments, even in the absence of the *parBS* complex. **(B)** The percentage of cells having cytoplasmic filaments was similar in the case of $ParA_F$ M315I Q351H-GFP [39.2 % ± 3.37 (95% CI, n=3; number of cells counted > 100 for each experiment)], $ParA_F$ Q351H-GFP [48.7 ± 9.5 (95% CI, n = 3; number of cells counted > 150 for each experiment)], $ParA_F$ W362E-GFP [42.8 ± 8.2 (95% CI, n = 3; number of cells counted > 150 for each experiment)] and $ParA_F$ W362A-GFP filaments [53.8 ± 15.1 (95% CI, n = 3; number of cells counted > 150 for each experiment)]. **(C)** Superplots showing the quantification of the length of the cytoplasmic filaments assembled by $ParA_F$ Q351H-GFP and $ParA_F$ W362E-GFP. No significant difference was observed with an average length of 0.88 μm ± 0.08 (SD, n = 3; number of cells counted > 73 < 121) in the case of $ParA_F$ Q351H-GFP and 0.71 μm ± 0.06 (SD, n = 3; number of cells counted > 59 < 99) in the case of $ParA_F$ W362E-GFP. $ParA_F$ and the various mutants described were expressed from the weak P_{trc} promoter in pDSW210 as C-terminal GFP fusions by the addition of 100 μM IPTG for 2 hours in *E. coli* MC4100. Cultures were grown to an OD_{600} of 0.2 before the addition of IPTG for protein expression. **(D)** *S. pombe* cultures carrying pREP42-$ParA_F$-GFP or $ParA_F$ mutants M315I Q351H, Q351H or W362E were grown in EMM medium in the absence of thiamine for 20 – 24 hours to allow for the expression of the $ParA_F$-GFP protein. $ParA_F$ localised to the nucleus (possibly by diffusion and retention due to DNA binding activity), and $ParA_F$

M315I Q351H-GFP (SopA1-GFP), $ParA_F$ Q351H-GFP and $ParA_F$ W362E-GFP assembled into polymers in the cytoplasm. Bacterial cells or yeast cells were mounted onto a 1.6% agarose slide and imaged using an epifluorescence microscope. A two-sided Student's -t-test was used to calculate P-values in the case of **(B and C)**. ns represents a p-value > 0.05. All experiments were repeated at least thrice (n = 3, three biological replicates). Error bars are inferential and represent the 95% confidence interval in **(B)** and represent the standard deviation (SD) of the mean in **(C)**. Scale bars represent 3 μm for all images.

Figure 3

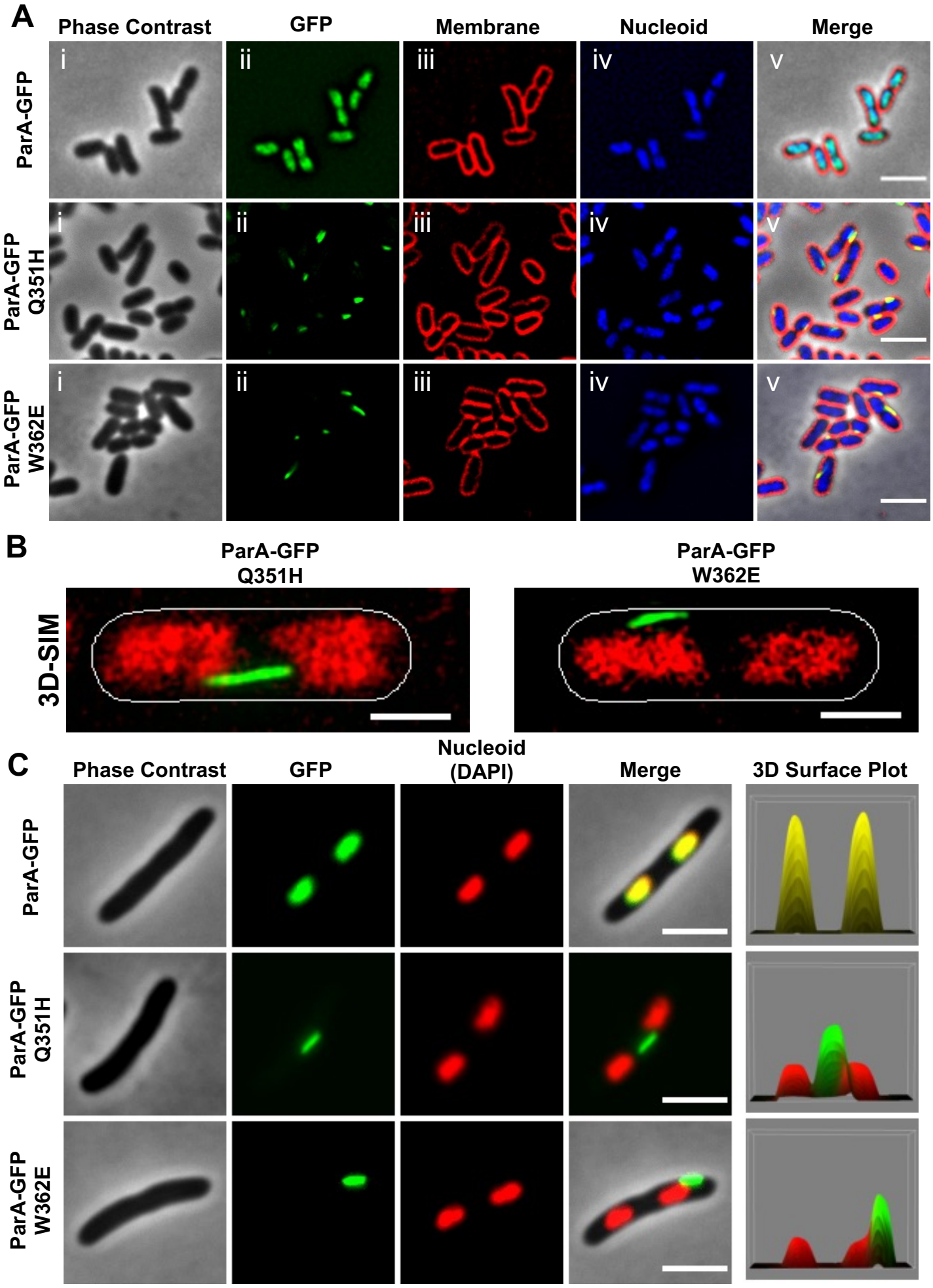
A
Phase Contrast
GFP
Membrane
Nucleoid
Merge
ParA-GFP
ParA-GFP Q351H
ParA-GFP W362E
i
ii
iii
iv
v
B
ParA-GFP Q351H
ParA-GFP W362E
3D-SIM
C
Phase Contrast
GFP
Nucleoid (DAPI)
Merge
3D Surface Plot
ParA-GFP
ParA-GFP Q351H
ParA-GFP W362E

Figure 3. Residues Q351 and W362 influence non-specific DNA binding by $ParA_F$.

(A) Filaments formed by $ParA_F$ Q351H-GFP and $ParA_F$ W362E-GFP are not nucleoid-associated. The $ParA_F$ Q351H-GFP and $ParA_F$ W362E-GFP filaments appeared to be localised in the space between the nucleoid and the inner membrane, while $ParA_F$-GFP localised over the nucleoids. Nucleoids were stained with DAPI, and the plasma membrane was stained using FM4-64. **(B)** Super-resolution imaging using 3D structured illumination microscopy (3D-SIM) showing the filaments assembled by **(i)** $ParA_F$ Q351H-GFP and **(ii)** $ParA_F$ W362E-GFP are not associated with the nucleoid. DNA was stained with DAPI and pseudo-coloured red. Cell outlines were obtained from the phase contrast images. **(C)** Filaments formed by $ParA_F$ Q351H-GFP and $ParA_F$ W362E-GFP are found in the nucleoid-free spaces in the cytoplasm of *E. coli*. Wild-type $ParA_F$-GFP localised to the nucleoid. Nucleoids were visualised by staining with DAPI and pseudo-coloured red in the images. Cells were treated with 25 µg/ mL cephalexin for 30 minutes to prevent cell division and 100 µg/ mL chloramphenicol for 10 minutes to condense the nucleoids so that the nucleoid-free space appears pronounced. Scale bars represent 3 µm in all images except in **(B)**, where the scale bar is 1 µm.

Figure 4

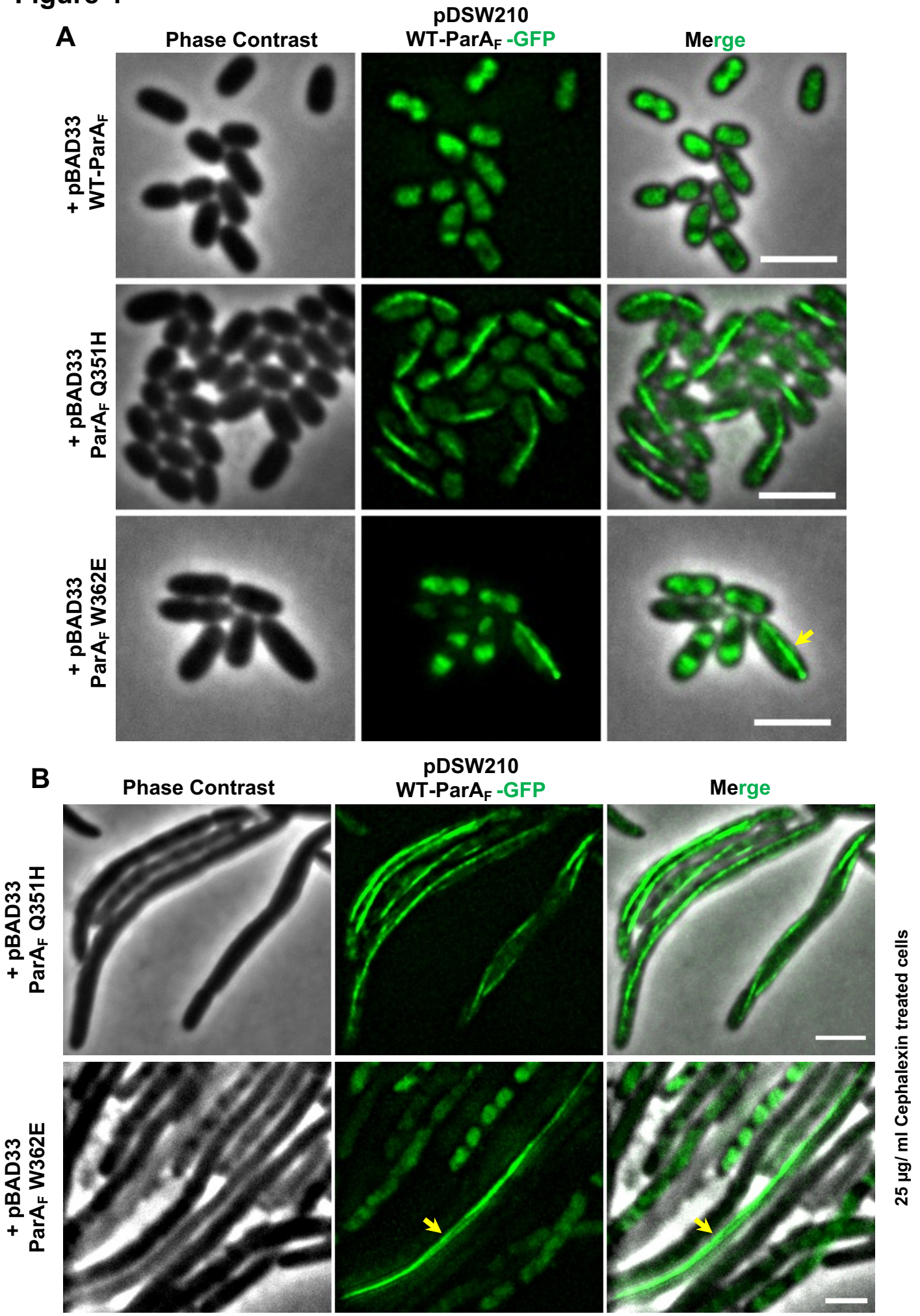
A
Phase Contrast
pDSW210
WT-ParA$_F$ -GFP
Merge
+ pBAD33
WT-ParA$_F$
+ pBAD33
ParA$_F$ Q351H
+ pBAD33
ParA$_F$ W362E
B
Phase Contrast
pDSW210
WT-ParA$_F$ -GFP
Merge
+ pBAD33
ParA$_F$ Q351H
+ pBAD33
ParA$_F$ W362E
25 µg/ ml Cephalexin treated cells

Figure 4. Filament-forming mutants of $ParA_F$ can induce the assembly of wild-type $ParA_F$-GFP into cytoplasmic filaments.

(A) Polymerisation of $ParA_F$-GFP upon co-expression of untagged $ParA_F$ Q351H or $ParA_F$ W362E. $ParA_F$-GFP localises to the nucleoid upon co-expression with untagged $ParA_F$, but co-expression of untagged $ParA_F$ Q351H induces the assembly of $ParA_F$-GFP into cytoplasmic filaments. Untagged $ParA_F$ W362E can also induce the polymerisation of $ParA_F$-GFP but is very inefficient compared to $ParA_F$ Q351H, and $ParA_F$-GFP remains predominantly nucleoid localised. **(B)** Assembly of $ParA_F$-GFP into long filaments in cephalexin-treated cells upon co-expression of untagged $ParA_F$ Q351H. $ParA_F$-GFP was expressed from the weak P_{trc} promoter of pDSW210 vector by the addition of 100 μM IPTG, and untagged versions of $ParA_F$, $ParA_F$ Q351H or $ParA_F$ W362E were co-expressed from the tightly regulated arabinose inducible promoter P_{BAD} from pBAD33 vector. Cells were treated with 25 μg/ mL cephalexin in **(B)** to obtain filamentous cells and inhibit cell division for better visualisation of $ParA_F$ filaments. Scale bars represent 2 μm.

Figure 5

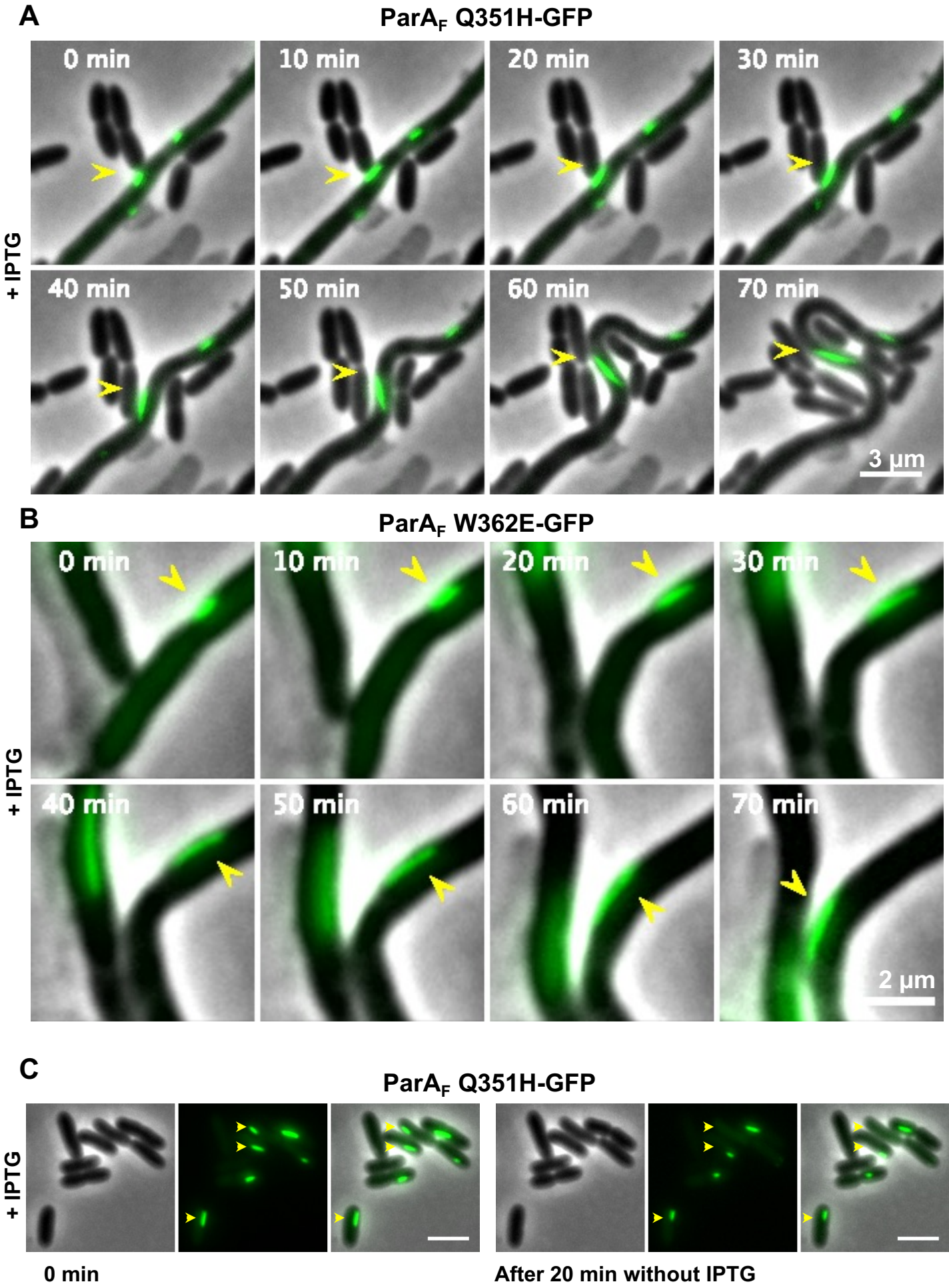
A
ParA$_F$ Q351H-GFP
+ IPTG
0 min
10 min
20 min
30 min
40 min
50 min
60 min
70 min
3 µm
B
ParA$_F$ W362E-GFP
+ IPTG
0 min
10 min
20 min
30 min
40 min
50 min
60 min
70 min
2 µm
C
ParA$_F$ Q351H-GFP
+ IPTG
0 min
After 20 min without IPTG

Figure 5

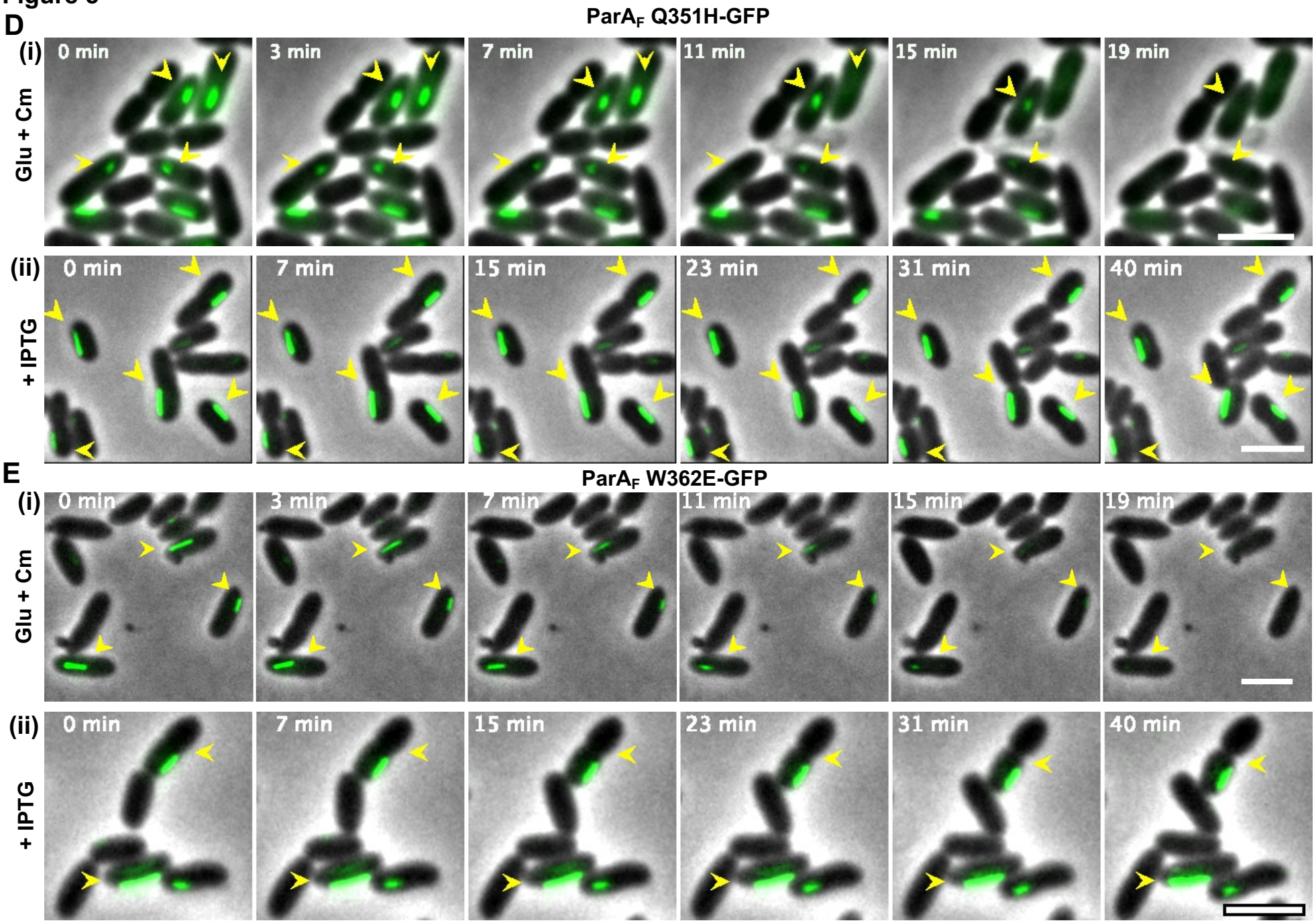
D
ParA$_F$ Q351H-GFP
(i)
Glu + Cm
0 min
3 min
7 min
11 min
15 min
19 min
(ii)
+ IPTG
0 min
7 min
15 min
23 min
31 min
40 min
E
ParA$_F$ W362E-GFP
(i)
Glu + Cm
0 min
3 min
7 min
11 min
15 min
19 min
(ii)
+ IPTG
0 min
7 min
15 min
23 min
31 min
40 min

Figure 5. Maintenance of $ParA_F$ Q351H and $ParA_F$ W362E polymers requires continuous protein synthesis in cells.

(A – B) Time-lapse images showing the growth of $ParA_F$ filaments formed by **(A)** $ParA_F$ Q351H-GFP and **(B)** $ParA_F$ W362E-GFP. Live cells were imaged on LB-agarose pads containing 100 μM IPTG and 25 μg/ mL cephalexin. Images were acquired every 10 minutes for a total of 70 minutes on a Delta Vision Elite™ microscope. Arrowheads depict the growing filaments. Cells were treated with cephalexin (25 μg/ mL) to prevent cell division to clearly visualise the growth of $ParA_F$ filaments. **(C)** $ParA_F$ Q351H-GFP filaments appear to shorten in the absence of the inducer IPTG. *E. coli* MC4100 cells carrying pDSW210-$ParA_F$ Q351H-GFP were induced 100 μM IPTG and then placed on LB-agarose slides without IPTG. Images were acquired immediately after placing the cells on agarose slides, and the same field was imaged again after 20 minutes. **(D and E)** Time-lapse images showing the depolymerisation of $ParA_F$ filaments assembled by **(D i)** $ParA_F$ Q351H-GFP and **(E i)** $ParA_F$ W362E-GFP in the absence of continued protein synthesis within a period of 20 minutes. Cultures were induced 100 μM IPTG for 2 hours prior to placing on LB-agarose pads and imaging. Chloramphenicol (50 μg/ mL) and 2 % glucose were added to the agarose pads to stop protein synthesis and repress the IPTG inducible promoter in the pDSW210 vector, respectively. Images were acquired every minute for a total of 20 minutes. **(D ii)** Time-lapse images of $ParA_F$ Q351H-GFP and **(E ii)** $ParA_F$ W362E-GFP showing the stable maintenance of filaments up to 40 minutes in the presence of continuous protein synthesis. Cultures were induced 100 μM IPTG for 2 hours prior to placing on LB-agarose pads and imaging. Cells were imaged on LB-

agarose pads containing 200 μM IPTG. Images were acquired every minute for a total of 40 minutes. Scale bars represent 3 μm.

Figure 6

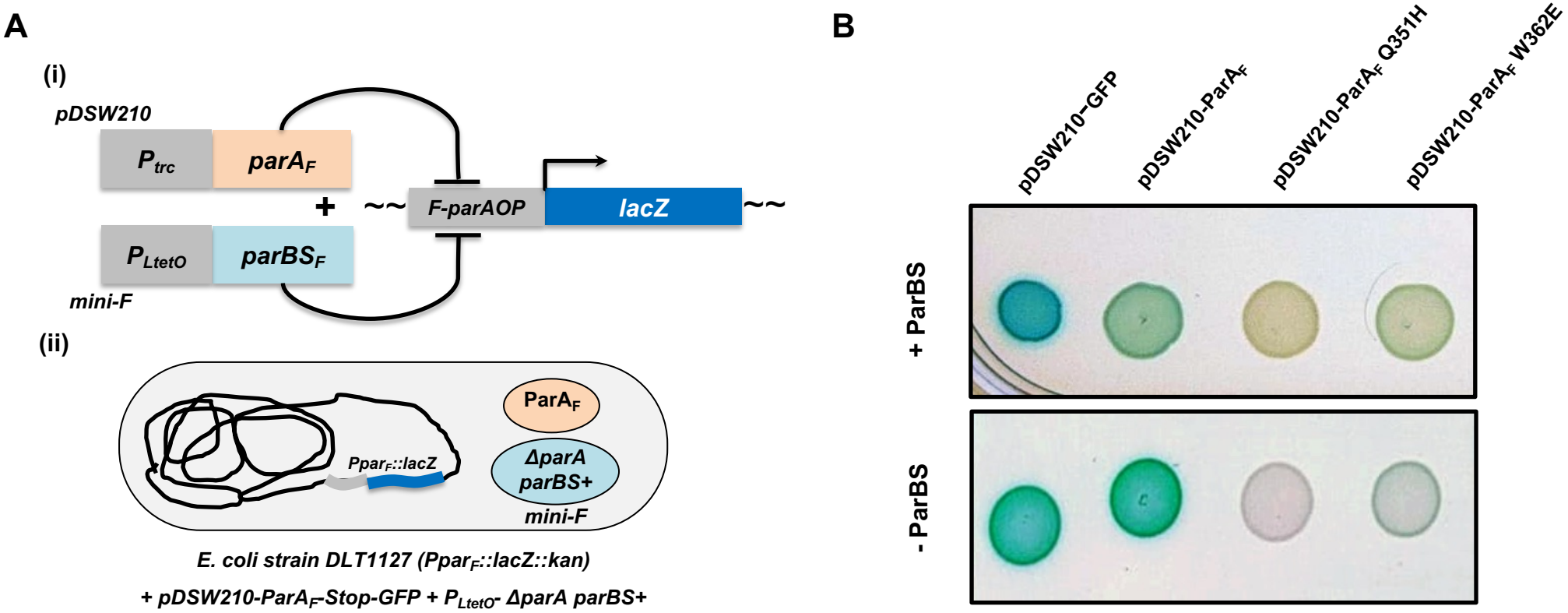
A
(i)
pDSW210
P_{trc}
$parA_F$
+
P_{LtetO}
$parBS_F$
mini-F
F-parAOP
lacZ
(ii)
$Ppar_F$::lacZ
$ParA_F$
ΔparA
parBS+
mini-F
E. coli strain DLT1127 ($Ppar_F$::lacZ::kan)
+ pDSW210-$ParA_F$-Stop-GFP + P_{LtetO}- ΔparA parBS+
B
pDSW210-GFP
pDSW210-$ParA_F$
pDSW210-$ParA_F$ Q351H
pDSW210-$ParA_F$ W362E
+ ParBS
- ParBS

Figure 6. $ParA_F$ Q351H and $ParA_F$ W362E act as transcriptional repressors of the ParA promoter and are independent of ParB

(A) Schematic showing the two-plasmid system and the LacZ-reporter strain used for determining the transcriptional repressor activity of $ParA_F$ in the presence or absence of ParBS complex. The strain DLT1127 carried the β-galactosidase gene *lacZ* under the promoter sequences of $ParA_F$. $ParA_F$ was expressed from the IPTG inducible weak P_{trc} promoter in the pDSW210 vector, and the ParB was expressed from the constitutive promoter P_{LtetO} and was carried on the mini-F plasmid lacking $parA_F$ (*ΔparA parBS*$^+$). $ParA_F$ acts to strongly repress the expression of *lacZ* from the P_{parA} promoter in the presence of ParB. **(B)** Qualitative β-galactosidase assay showing $ParA_F$ Q351H and $ParA_F$ W362E acting as super-repressors of the P_{parA} promoter by strongly preventing LacZ expression even in the absence of ParB. While cultures carrying vector control (expressing GFP) did not repress LacZ expression either in the presence or absence of ParBS, $ParA_F$ strongly reduced the expression of LacZ only in the presence of the ParBS complex (top panel). $ParA_F$ Q351H and $ParA_F$ W362E acted independently of ParB and strongly repressed LacZ expression in the absence of ParB as well (bottom panel). Cultures of *E. coli* strain DLT1127 carrying pDSW210-GFP, pDSW210-$ParA_F$, pDSW210-$ParA_F$ Q351H or pDSW210-$ParA_F$ W362E were spotted on LB-agar plates containing appropriate antibiotics, 200 μM IPTG and 40 μM X-Gal and incubated overnight and imaged with CCD colour camera on a phone. Images were colour-corrected using the white-balance plugin in ImageJ v-1.54f.

Figure 7

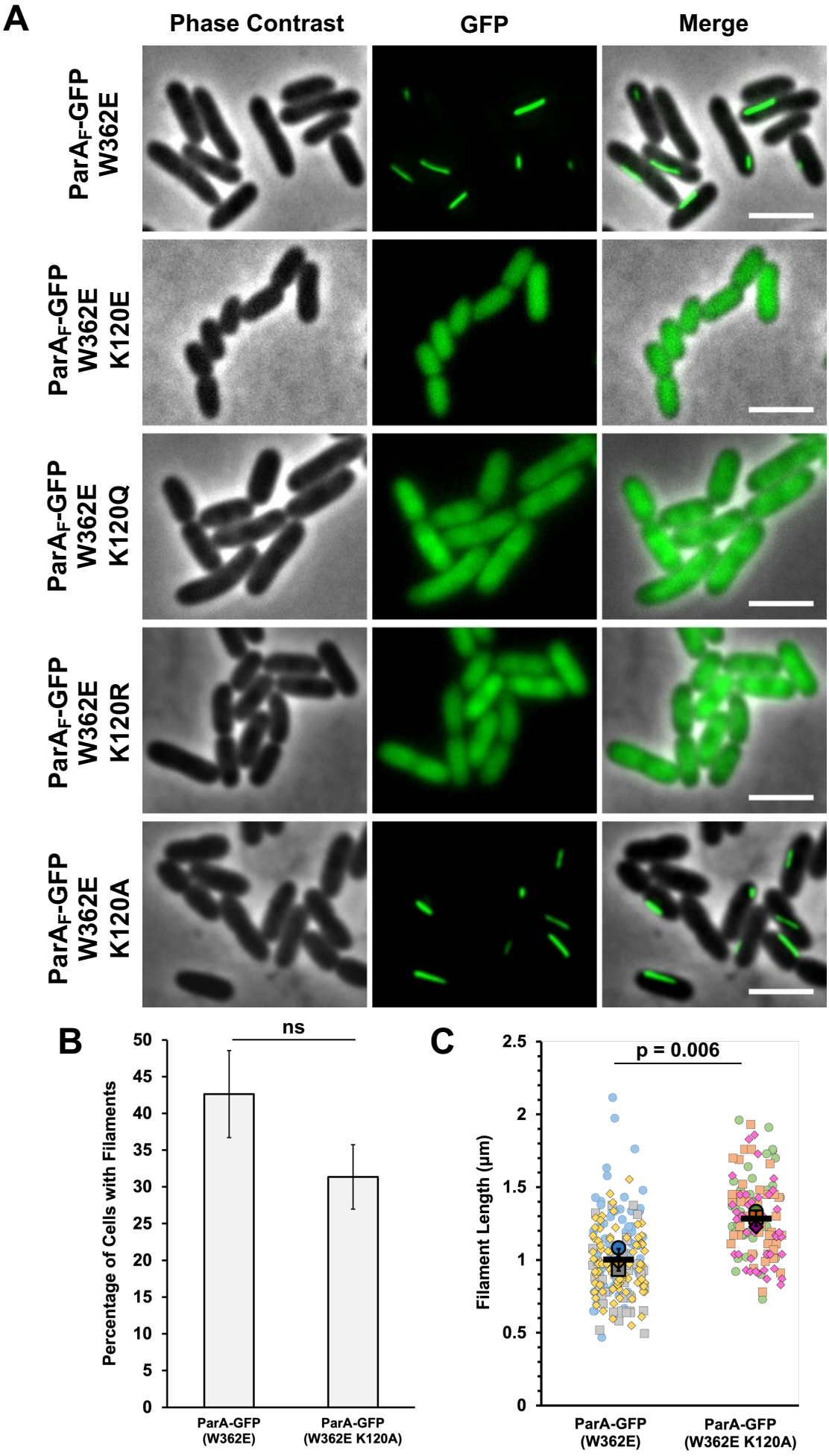
A
Phase Contrast
GFP
Merge
ParAF-GFP W362E
ParAF-GFP W362E K120E
ParAF-GFP W362E K120Q
ParAF-GFP W362E K120R
ParAF-GFP W362E K120A
B
ns
Percentage of Cells with Filaments
50
45
40
35
30
25
20
15
10
5
0
ParA-GFP (W362E)
ParA-GFP (W362E K120A)
C
p = 0.006
Filament Length (µm)
2.5
2
1.5
1
0.5
0
ParA-GFP (W362E)
ParA-GFP (W362E K120A)

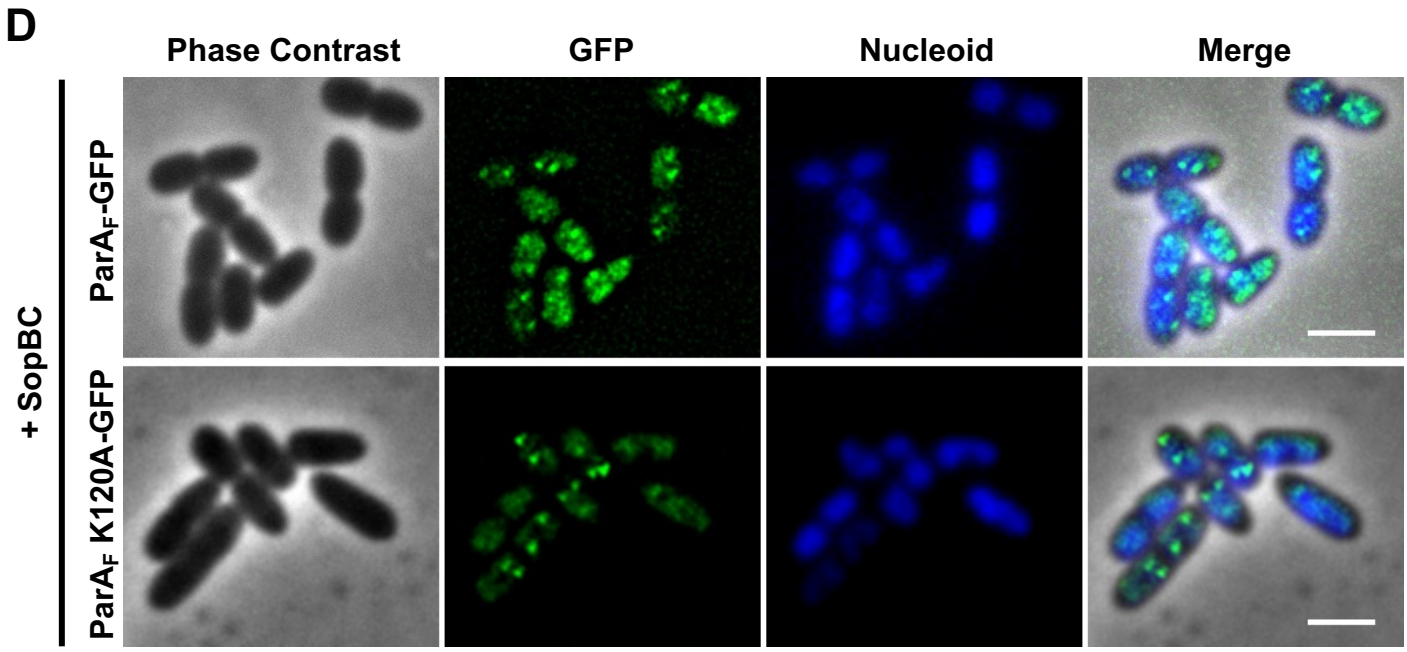
D
Phase Contrast
GFP
Nucleoid
Merge
+ SopBC
ParAF-GFP
ParAF K120A-GFP

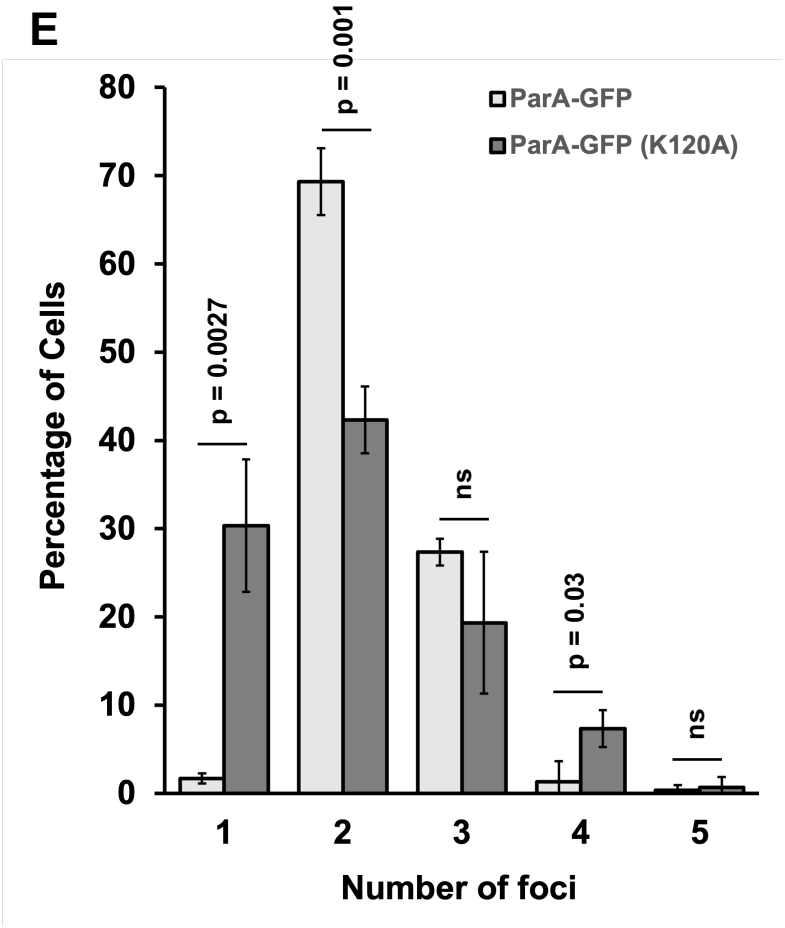
E
ParA-GFP
ParA-GFP (K120A)
Percentage of Cells
Number of foci
p = 0.0027
p = 0.001
ns
p = 0.03
ns
0
10
20
30
40
50
60
70
80
1
2
3
4
5

Figure 7. Filament assembly by $ParA_F$ W362E-GFP requires ATP-binding and the conformation change to the $ParA_F$-ATP* state

(A) Images showing the effect of various mutations in the conserved K120 residue on the polymerisation by $ParA_F$ W362E-GFP. While $ParA_F$ W362E-GFP assembles into cytoplasmic filaments, the introduction of K120E, which abolishes ATP binding in $ParA_F$, fails to form polymers. The introduction of K120R, which retains the ATP binding but does not hydrolyse ATP, also fails to form filaments. However, the introduction of K120Q, which retains the basal ATP hydrolysis, also fails to form filaments. Although $ParA_F$ K120R and $ParA_F$ K120Q bind the nucleotide, both are defective in achieving the conformational change to $ParA_F$-ATP* state upon interaction with ATP, thus showing that $ParA_F$-ATP* state is important for the polymerisation of $ParA_F$ W362E-GFP. Changing K120 to alanine in $ParA_F$ W362E did not affect the filament assembly. **(B)** Quantification of the percentage of cells having cytoplasmic filaments in the $ParA_F$-W362E-GFP and $ParA_F$-W362E K120A-GFP. While in the case of $ParA_F$-W362E-GFP, 42.6 % ± 5.9 (SD, n = 3, at least a total of 150 cells were counted for each experiment) cells had polymers, 31.3 % ± 4.4 (SD, n = 3, at least a total of 150 cells were counted for each experiment) of cells had filaments in the case of $ParA_F$-W362E K120A-GFP and were not significantly different. The differences were not statistically significant and had a p-value > 0.05. **(C)** Superplots showing the quantification of the filament lengths in the $ParA_F$-W362E-GFP and $ParA_F$-W362E K120A-GFP. While in the case of $ParA_F$-W362E-GFP, the average length of the filament was 1.0 µm ± 0.08 (SD, n = 3, total number of cells counted were > 75 < 84 for each replicate), $ParA_F$-W362E K120A-GFP exhibited an average polymer length of 1.28 % ± 0.05 (SD, n = 3, total number of cells counted were > 40 < 42 for each replicate). The

effect size was 0.28 [0.14, 0.43]. **(D)** $ParA_F$ K120A-GFP interacts with the partitioning complex, ParBS and forms cloud-like structures and foci over the bacterial nucleoid similar to $ParA_F$-GFP, suggesting that K120A mutation allows the conformational change to the $ParA_F$-ATP* state and does not affect ATP-binding or nsDNA binding of $ParA_F$. **(E)** Quantification of the number of foci assembled per cell by $ParA_F$-GFP and $ParA_F$ K120A-GFP. A greater percentage of cells have single-foci in the case of $ParA_F$ K120A-GFP [30.3 ± 7.5 (SD, n = 3, a total of 100 cells were counted for each replicate)] as compared to $ParA_F$-GFP [1.7 ± 0.6 (SD, n = 3, a total of 100 cells were counted for each replicate)]. ns represents non-significant. The error bars in the graphs represent the standard deviation of the mean (SD), and the scale bars in the images represent 2 μm.

Figure 8

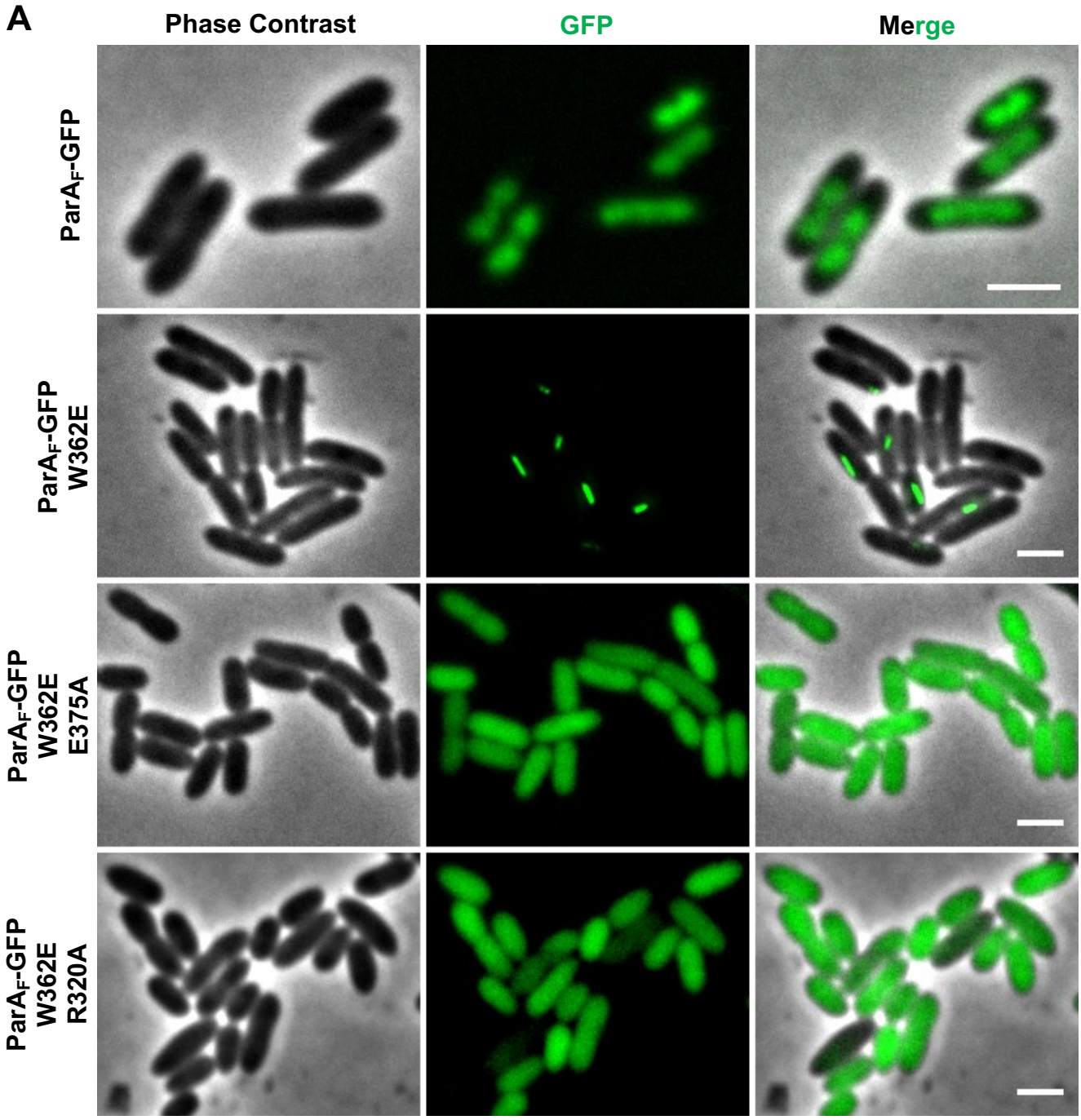
A
Phase Contrast
GFP
Merge
ParAF-GFP
ParAF-GFP W362E
ParAF-GFP W362E E375A
ParAF-GFP W362E R320A

Figure 8

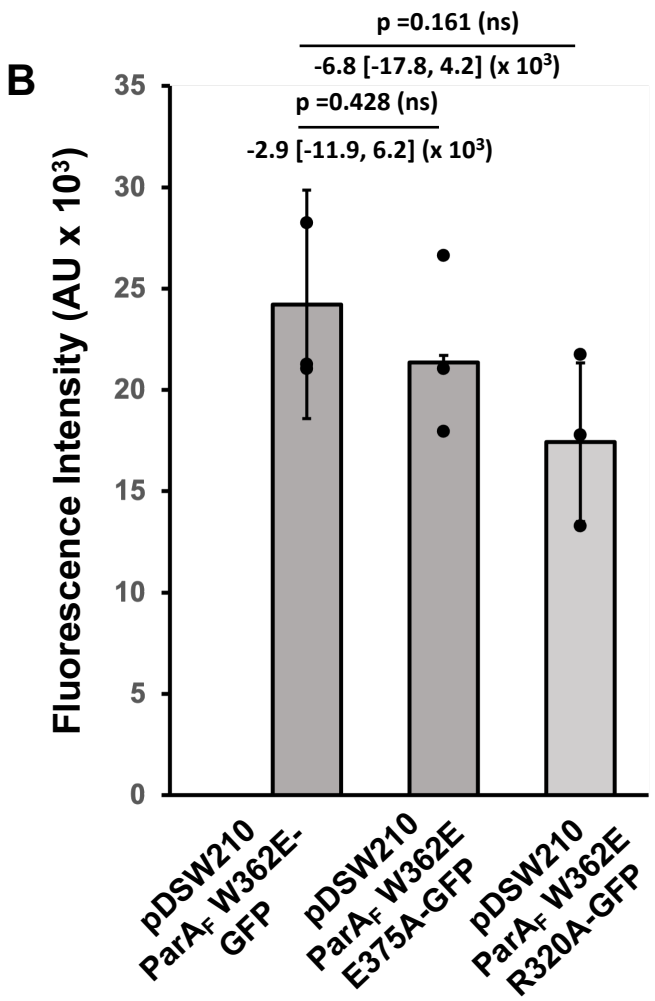
B
p =0.161 (ns)
-6.8 [-17.8, 4.2] (x 10³)
p =0.428 (ns)
-2.9 [-11.9, 6.2] (x 10³)
Fluorescence Intensity (AU x 10³)
35
30
25
20
15
10
5
0
pDSW210 ParAF W362E-GFP
pDSW210 ParAF W362E E375A-GFP
pDSW210 ParAF W362E R320A-GFP

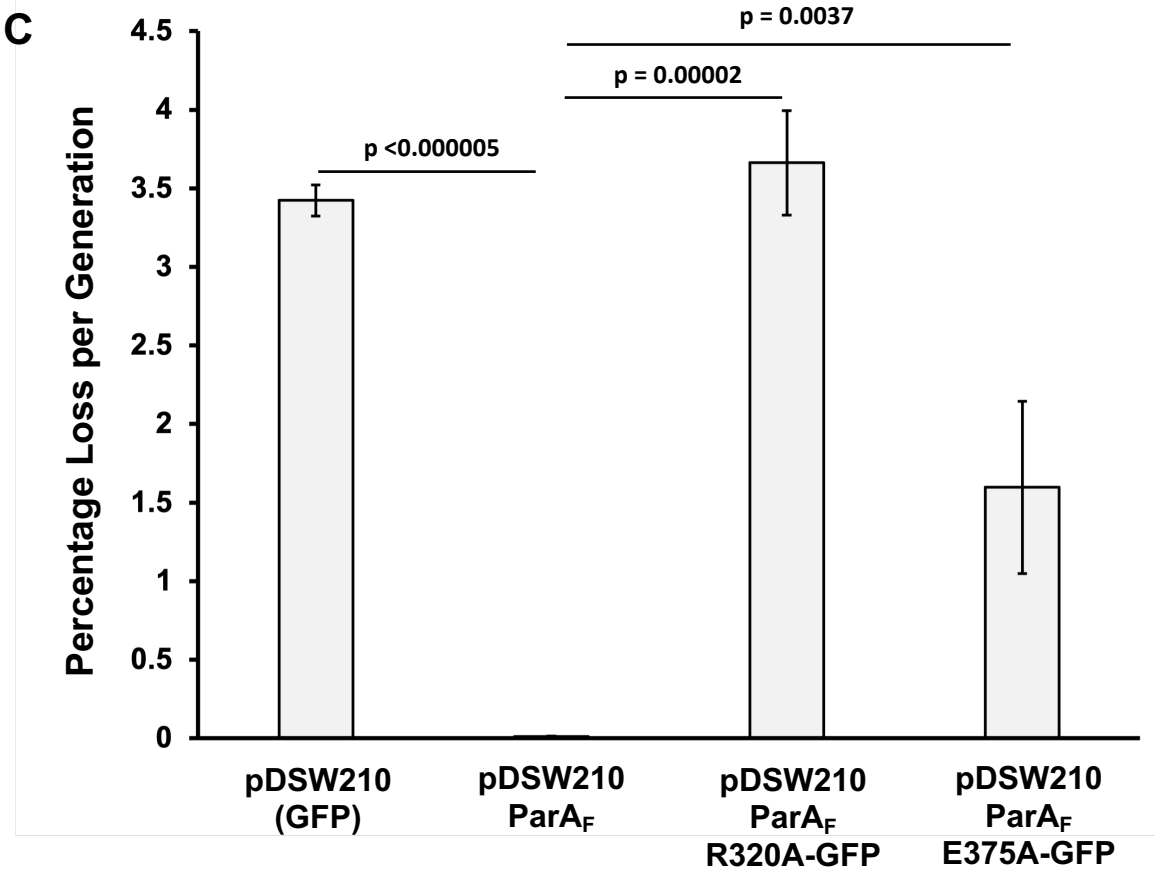
C
p = 0.0037
p = 0.00002
p <0.000005
Percentage Loss per Generation
4.5
4
3.5
3
2.5
2
1.5
1
0.5
0
pDSW210 (GFP)
pDSW210 ParAF
pDSW210 ParAF R320A-GFP
pDSW210 ParAF E375A-GFP

Figure 8

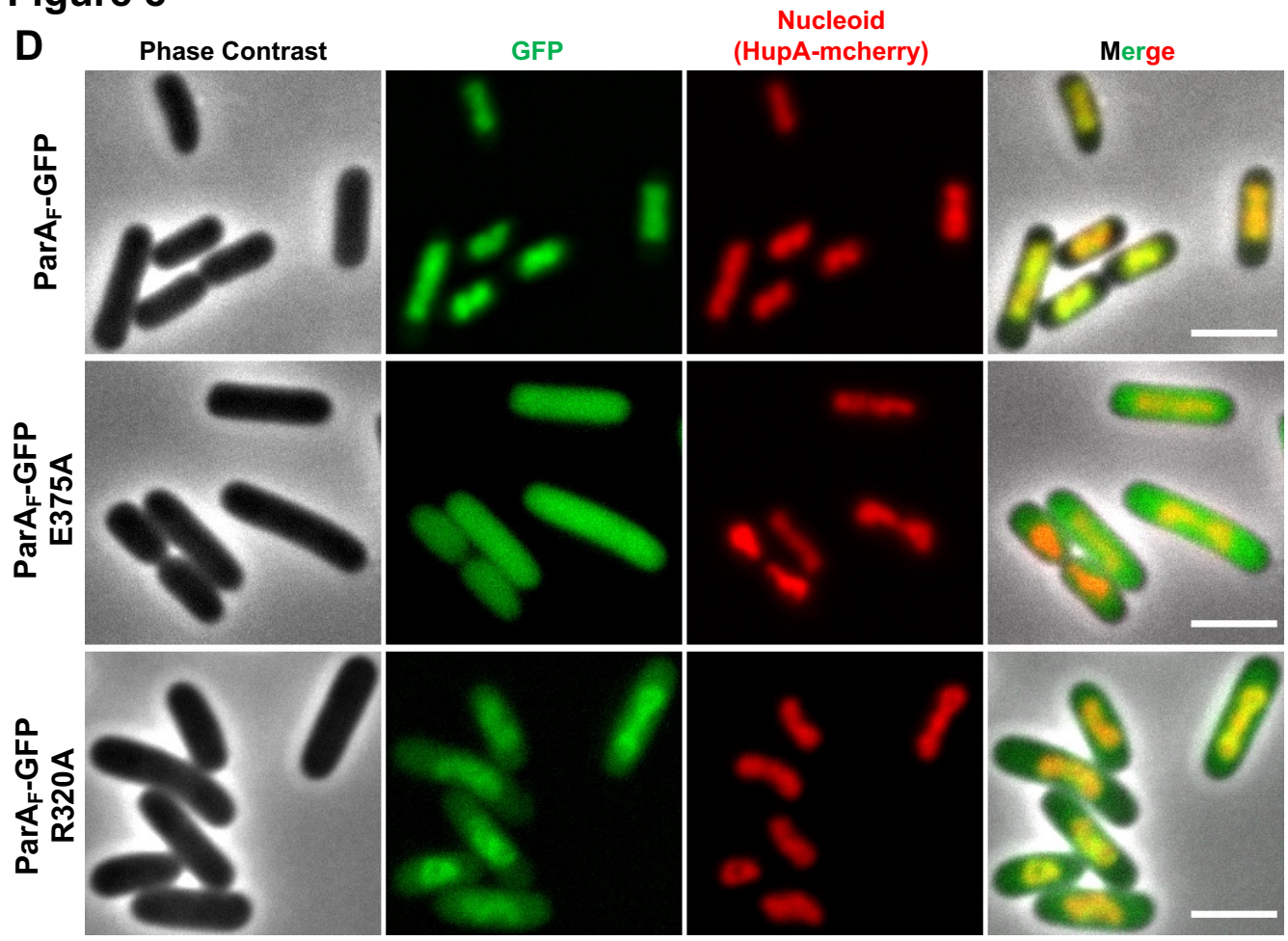
D
Phase Contrast
GFP
Nucleoid
(HupA-mcherry)
Merge
ParAF-GFP
ParAF-GFP
E375A
ParAF-GFP
R320A

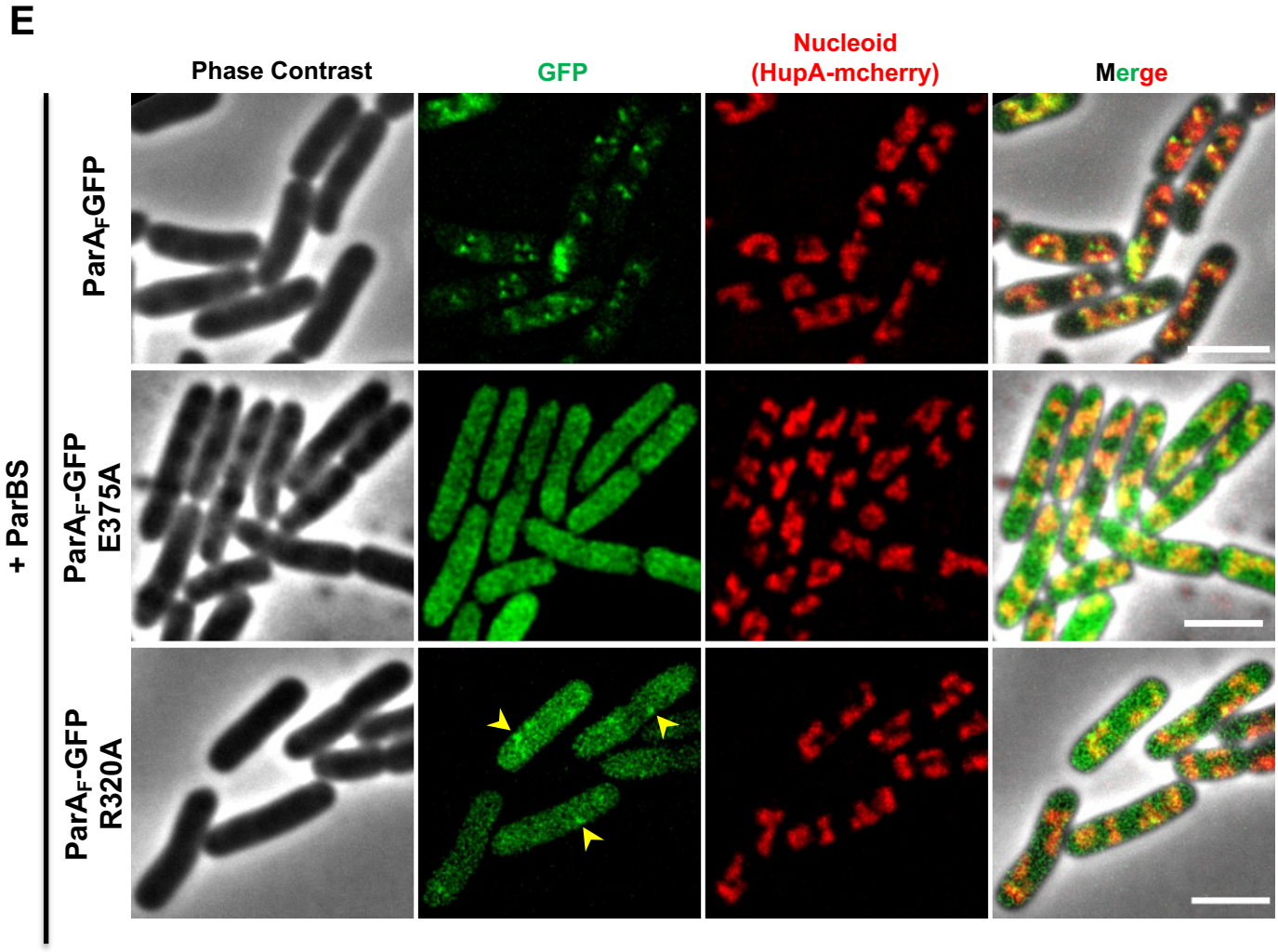
E
Phase Contrast
GFP
Nucleoid
(HupA-mcherry)
Merge
+ ParBS
ParAFGFP
ParAF-GFP
E375A
ParAF-GFP
R320A
Deconvolved Images

Figure 8. Identification of E375 in helix 16 and R320 in helix 14 as possible interface residues critical for polymerisation of $ParA_F$.

(A) While $ParA_F$ W362E-GFP assembles into filaments, introducing either E375A or R320A abolishes polymerisation. **(B)** Quantification of the total fluorescence intensities (sum intensity) in cells expressing $ParA_F$ W362E-GFP, $ParA_F$ W362E E375A-GFP or $ParA_F$ W362E R320A-GFP showing no significant differences in protein levels. Mean values from three independent biological replicates (N=3, number of cells counted was>400 for each replicate) are plotted. The values from the replicates are shown as black dots, and the mean value is plotted as a bar, with the SD values as the error bars. The p-values and the effect size are mentioned. The effect size is given as the difference in the means, and the 95% CI is indicated within parentheses. **(C)** Cultures expressing $ParA_F$ W362E E375A-GFP or $ParA_F$ W362E R320A-GFP fail to main the mini-F plasmids (*ΔparA*, *parBS*$^+$) unlike cells expressing WT-$ParA_F$-GFP. Error bars represent SD values. **(D)** Unlike $ParA_F$-GFP, which co-localises with the bacterial nucleoid, $ParA_F$ E375A-GFP and $ParA_F$ R320A-GFP are distributed in the cytoplasm. However, $ParA_F$ R320A-GFP shows mild localisation on the nucleoids compared to $ParA_F$ E375A-GFP. **(E)** In the presence of the partitioning complex, $ParA_F$ E375A-GFP fails to form foci and remains distributed throughout the cytoplasm, but $ParA_F$ R320A-GFP shows weak foci formation. $ParA_F$-GFP, as expected, appears as a haze or foci. An *E. coli* MG1655 derivative strain expressing carrying HupA-mCherry from its chromosomal locus was used to visualise the nucleoid, and cultures were induced with 100 μM IPTG for 2 hours to allow for the expression of $ParA_F$-GFP, $ParA_F$ E375A-GFP or $ParA_F$ R320A-GFP from the pDSW210 vector. Scale bars represent 2 μm.

Figure 9

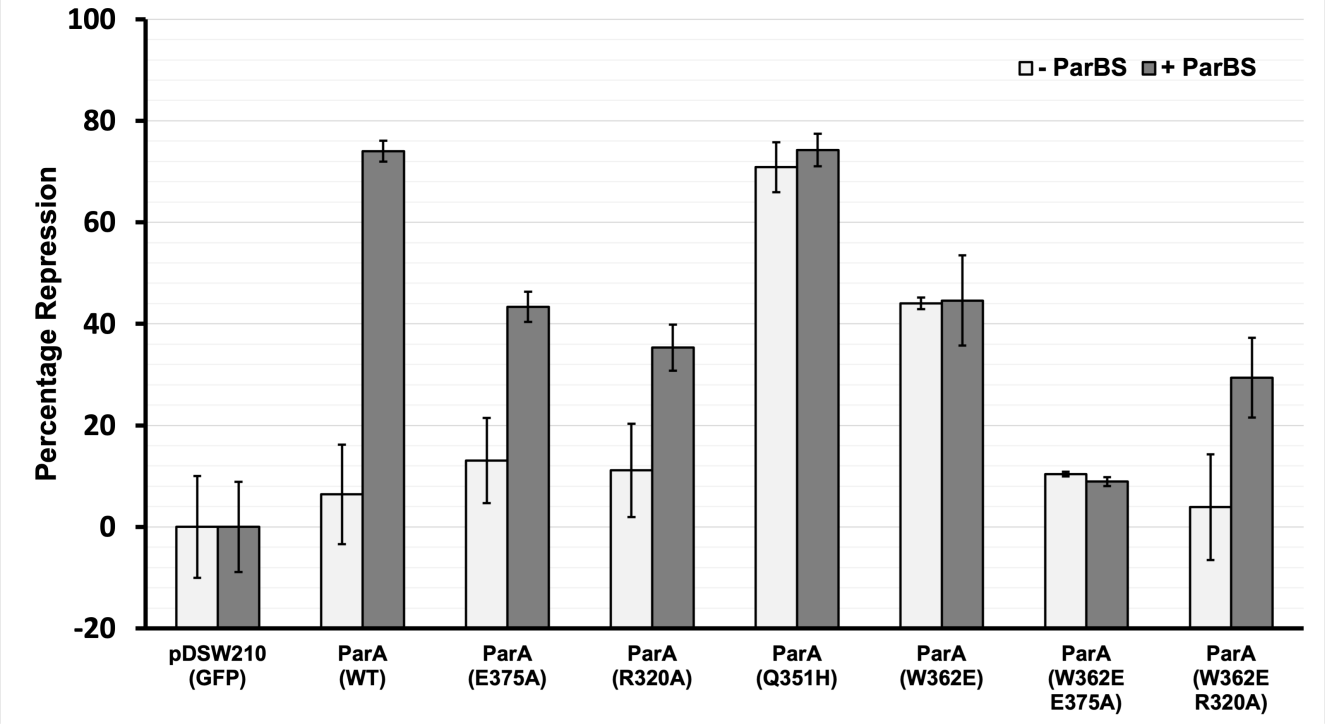
100
80
60
40
20
0
-20
Percentage Repression
- ParBS
+ ParBS
pDSW210 (GFP)
ParA (WT)
ParA (E375A)
ParA (R320A)
ParA (Q351H)
ParA (W362E)
ParA (W362E E375A)
ParA (W362E R320A)

Figure 9. E375A and R320A mildly compromise the repressor activity of $ParA_F$ but remain responsive to the $ParBS_F$ partitioning complex.

Quantitative β-galactosidase assay showing the repression activity by $ParA_F$ and the various mutants on the P_{parA} promoter. While the repression of $ParA_F$ is enhanced by the presence of the ParBS complex, $ParA_F$ Q351H-GFP and $ParA_F$ W362E-GFP strongly repress even in the absence of the ParB. Like $ParA_F$, $ParA_F$ E375A and $ParA_F$ R320A show increased repression activity in the presence of the ParBS complex than in the absence of ParBS, albeit to a lesser extent compared to wild-type $ParA_F$. The introduction of E375A or R320A mutations into $ParA_F$ W362E also drastically reduces their ability to repress LacZ expression. Miller units were calculated as described in the materials and methods section, and the values obtained were normalised with respect to the vector control, pDSW210-GFP. Further, since the expression of LacZ in the vector control culture (in the absence of $ParA_F$) was the maximum, normalised Miller units obtained in the case of pDSW210-GFP were considered as 100 % expressed or as 0 % repressed. Error bars represent the standard deviation of the mean (SD). Statistical significance test on the effect of ParBS on the repression activity was carried out using the estimated p-values from a one-tailed Student's t-test (since repression values are only expected to be higher in the presence of ParBS) and are indicated in the graph.

Figure 10

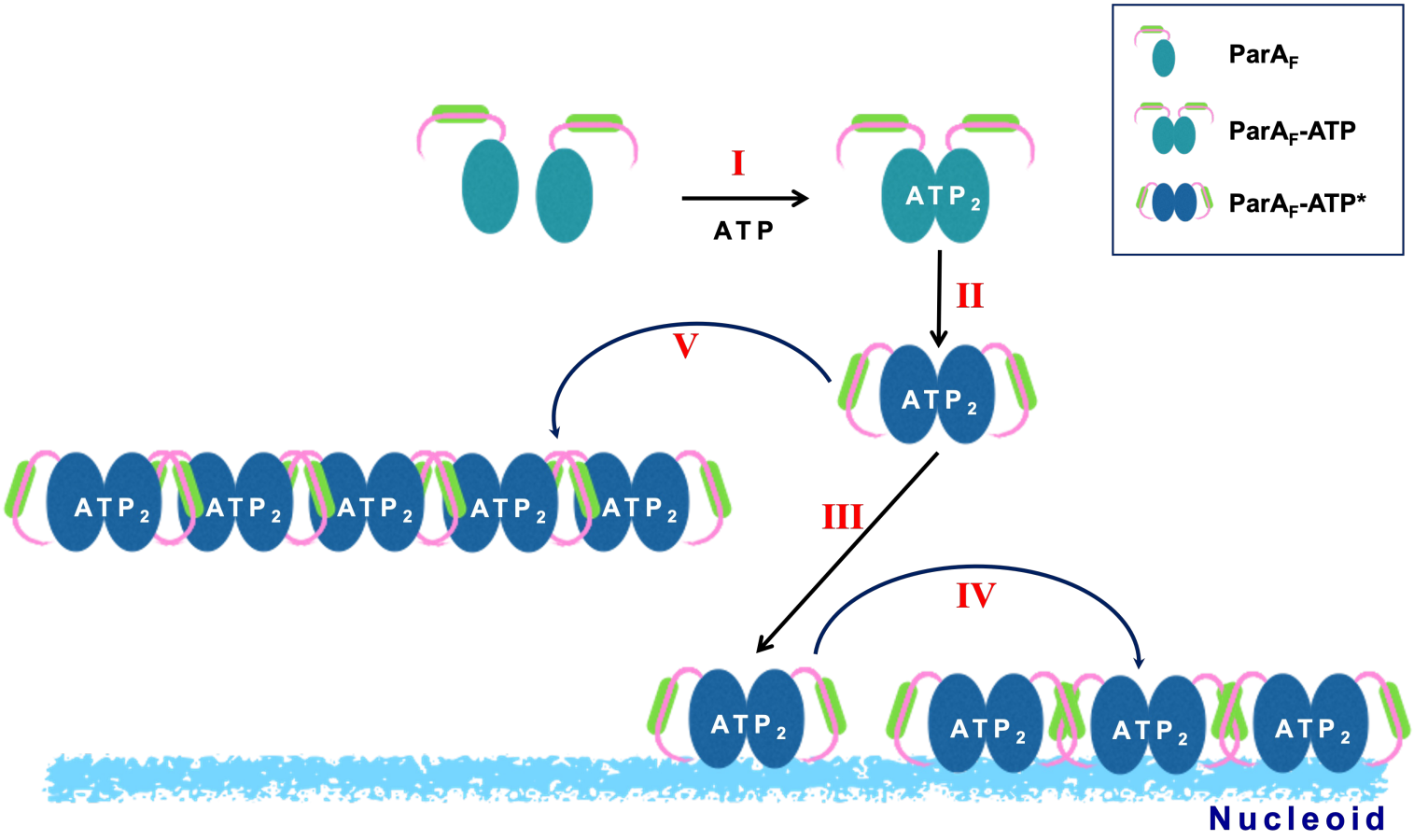

ParA$_F$ Protein	Function (Step) Affected				
	I	II	III	IV	V
Wild-type ParA$_F$	✓	✓	✓	✓	--
ParA$_F$ Q351H	✓	✓	X	X	✓
ParA$_F$ W362E	✓	✓	X	X	✓
ParA$_F$ R320A	✓	x	X	X	--
ParA$_F$ E375A	✓	X	X	X	--
ParA$_F$ W362E R320A	--	--	X	X	X
ParA$_F$ W362E E375A	--	--	X	X	X

Figure 10. Schematic showing the effect of various mutations on the oligomerisation of $ParA_F$ protein.

Monomeric apo-$ParA_F$ binds ATP to form the ATP sandwich dimer and undergoes a conformational change, resulting in the $ParA_F$-ATP* state. The $ParA_F$-ATP* binds the bacterial nucleoid as an ATP sandwich dimer, which could further undergo cooperative binding involving transient oligomerisation. The various steps are marked in roman numerals and the effect of various mutations is tabulated. A tick mark (✔) shows activity, a small cross mark shows (x) partial impairment of activity and a cross mark (X) shows the step likely affected by the mutation. The mutations Q351H and W362E result in the formation of stable cytoplasmic filaments that are incompatible with nsDNA binding (nucleoid localisation). The mutations in the C-terminal helix-14 (R320A) or helix-16 (E375A) abolish oligomerisation. The mutations R320A and E375A might possibly inhibit polymerisation either by blocking direct subunit interactions or preventing the conformational change to the $ParA_F$-ATP* state.

Table 1

(i)

ParA	Effect Size (ParA)	P-value (1-tailed)	Effect Size (ParA)	P-value (1-tailed)
	- ParBS		+ ParBS	
ParA W362E	NA	NA	NA	NA
ParA W362E E375A	**-33.6 [-36.5, -30.8]**	**0.00002**	**-35.7 [-56.8, -14.6]**	**0.00628**
ParA W362E R320A	**-40.1 [-57.8, -22.4]**	**0.00275**	-15.2 [-40, 9.6]	0.07322

(ii)

ParA	Effect Size (ParA)	P-value (1-tailed)	Effect Size (ParA)	P-value (1-tailed)
	- ParBS		+ ParBS	
ParA	NA	NA	NA	NA
ParA E375A	6.7 [-11.5, 24.8]	0.21140	**-30.7 [-43.7, -17.6]**	**0.00006**
ParA R320A	4.7 [-14.2, 23.6]	0.28783	**-38.7 [-52.6, -24.8]**	**0.00009**

(iii)

ParA	Effect Size (pDSW210)	P-value (1-tailed)	Effect Size (ParA)	P-value (1-tailed)	Effect Size (pDSW210)	P-value (1-tailed)	Effect Size (ParA)	P-value (1-tailed)	Effect Size (ParBS)	P-value (1-tailed)
	- ParBS				+ ParBS					
pDSW210-GFP	NA	NA	--	--	NA	NA	--	--	NA	NA
ParA	6.4 [-13.1, 25.9]	0.23681	NA	NA	**74 [61.3, 86.7]**	**0.00007**	NA	NA	**67.6 [51.5, 83.7]**	**0.00015**
ParA E375A	13.1 [-5.1, 31.2]	0.07939	6.7 [-11.5, 24.8]	0.21140	**43.4 [30.3, 56.4]**	**0.00066**	**-30.7 [-43.7, -17.6]**	**0.00006**	**30.3 [16, 44.6]**	**0.00209**
ParA R320A	11.1 [-7.8, 30]	0.11471	4.7 [-14.2, 23.6]	0.28783	**35.3 [21.5, 49.2]**	**0.00180**	**-38.7 [-52.6, -24.8]**	**0.00009**	**24.2 [7.7, 40.6]**	**0.00754**
ParA Q351H	**70.8 [55.3, 86.4]**	**0.00020**	**64.4 [48.9, 80]**	**0.00027**	**74.3 [61.1, 87.4]**	**0.00009**	0.2 [-12.9, 13.4]	0.46074	3.4 [-6, 12.9]	0.18623
ParA W362E	**44 [30, 58]**	**0.00082**	**37.6 [23.6, 51.6]**	**0.00138**	**44.6 [27.1, 62.1]**	**0.00178**	**-29.4 [-46.9, -12]**	**0.00250**	0.6 [-13.8, 14.9]	0.45868
ParA W362E E375A	10.4 [-13.4, 34.2]	0.12910	4 [-19.3, 27.3]	0.31173	8.9 [-12.3, 30.1]	0.13652	**-65.1 [-70.2, -60.1]**	**0.00002**	-1.5 [-4.4, 1.4]	0.07948
ParA W362E R320A	3.9 [-25.6, 33.4]	0.35112	-2.5 [-31.6, 26.6]	0.40120	**29.4 [4.5, 54.3]**	**0.01650**	**-44.6 [-58.7, -30.6]**	**0.00103**	25.5 [-14.2, 65.2]	0.05498

Table 1. Table showing the statistical analysis of the quantitative β-galactosidase assays for estimating promoter repression activity by the various $ParA_F$ mutants.

The table shows the statistical analysis for the repression activity by various $ParA_F$ mutants in comparison to the vector control (pDSW210-GFP) or with $ParA_F$, where the repression was normalised to 0 %. Estimation statistics were also used to assess the statistical significance of the repressor functions. Effect size is defined as the difference between the means of samples being compared, and the 95 % CI of the difference is given within the square parentheses. Statistical analysis showing the p-values and effect size, along with the 95 % CI of the difference, is tabulated. **(i)** Statistical analysis for the repression activity by $ParA_F$ W362E E375A and $ParA_F$ W362E R320A in comparison to $ParA_F$ W362E showing the effect size along with the 95 % CI of the difference. The double mutants $ParA_F$ W362E E375A and $ParA_F$ W362E R320A show reduced repression of the P_{parA} promoter than $ParA_F$ W362E with an effect size of -33.6 [-36.5, -30.8] and -40.1 [-57.8, -22.4], respectively. **(ii)** In the presence of ParBS, $ParA_F$ E375A and $ParA_F$ R320A show a reduced repression activity than the WT-$ParA_F$ with an effect size of -30.7 [-43.7, -17.6] and -38.7 [-52.6, -24.8], respectively. **(iii)** Table shows the statistical analysis for the repression activity by various $ParA_F$ mutants in comparison to the vector control (pDSW210-GFP). The effect size and the 95 % CI of the difference in the absence of ParBS as well as in the presence of ParBS are tabulated. In the absence of ParBS, $ParA_F$ Q351H and $ParA_F$ W362E act as super-repressors, showing an effect size of 70.8 [55.3, 86.4] and 44 [30, 58], respectively compared to pDSW210-GFP. When compared to $ParA_F$, $ParA_F$ Q351H and $ParA_F$ W362E show an effect size of 64.4 [48.9, 80] and 37.6 [23.6, 51.6], respectively. The statistical significance of the results for the effect of the

ParBS complex is also tabulated. Although $ParA_F$ E375A and $ParA_F$ R320A have reduced repression in the presence of ParBS compared to $ParA_F$, they are responsive to ParB and their ability to repress is still enhanced by the presence of the ParBS complex. While $ParA_F$ shows an effect size of 67.6 [51.5, 83.7], $ParA_F$ E375A and $ParA_F$ R320A show an effect size of 30.3 [16, 44.6] and 24.2 [7.7, 40.6], respectively. Results that are deemed statistically significant are shown in bold. P-values were obtained from a one-tailed Student's t-test (since repression values are expected to be only higher (0 % or greater than experimental samples lacking ParBS). P-values ≥ 0.05 (after rounding off to 2 decimals) were considered statistically non-significant. Effect sizes are easier to interpret, with negative values indicating reduced repression ability and positive values indicating increased repression than the test sample. The 95 % CI of the difference, when not encompassing zero, indicates a statistically significant difference.